Research Paper

THEMED ISSUE: Cenozoic Tectonics, Magmatism, and Stratigraphy of the Snake River Plain–Yellowstone Region and Adjacent Areas

GEOSPHERE

GEOSPHERE; v. 14, no. 1

doi:10.1130/GES01553.1

12 figures; 2 tables; 1 supplemental file

CORRESPONDENCE: brueseke@ksu.edu

CITATION: Brueseke, M.E., Downey, A.C., Dodd, Z.C., Hart, W.K., Adams, D.C., and Benowitz, J.A., 2017, The leading wisps of Yellowstone: Post–ca. 5 Ma extension-related magmatism in the upper Wind River Basin, Wyoming (USA), associated with the Yellowstone hotspot tectonic parabola: Geosphere, v. 14, no. 1, doi:10.1130/GES01553.1.

Science Editor: Shanaka de Silva
Associate Editor: Ben Ellis

Received 3 May 2017
Revision received 8 September 2017
Accepted 24 October 2017

GOLD OPEN ACCESS

THE GEOLOGICAL SOCIETY OF AMERICA®

This paper is published under the terms of the CC-BY-NC license.

© 2017 The Authors

The leading wisps of Yellowstone: Post–ca. 5 Ma extension-related magmatism in the upper Wind River Basin, Wyoming (USA), associated with the Yellowstone hotspot tectonic parabola

Matthew E. Brueseke[1], Anna C. Downey[1], Zachary C. Dodd[1], William K. Hart[2], Dave C. Adams[3], and Jeff A. Benowitz[4]

[1]Department of Geology, Kansas State University, 108 Thompson Hall, Manhattan, Kansas 66506, USA
[2]Department of Geology and Environmental Earth Science, Miami University, 118C Shideler Hall, Oxford, Ohio 45056, USA
[3]Box 155, Teton Village, Wyoming 83025, USA
[4]Geophysical Institute and Geochronology Laboratory, University of Alaska Fairbanks, Fairbanks, Alaska 99775, USA

ABSTRACT

The upper Wind River Basin in northwest Wyoming (USA) is located ~80–100 km southeast of the Yellowstone Plateau volcanic field. While the upper Wind River Basin is a manifestation of primarily Cretaceous to Eocene Laramide tectonics, younger events have played a role in its formation, including Eocene Absaroka volcanism, Cenozoic lithospheric extension, and the migration of the North American plate over the Yellowstone hotspot tail. New $^{40}Ar/^{39}Ar$ ages coupled with existing K-Ar results from intrusives and lavas in the upper Wind River Basin show that igneous activity younger than ca. 5 Ma occurred locally. Field and geochemical data show that these <ca. 5 Ma upper Wind River Basin magmas were either erupted or emplaced along normal fault zones at different locations and range in composition from tholeiitic basalt (Spring Mountain) to calc-alkaline basaltic andesite through dacite (Lava Mountain, Crescent Mountain, and Wildcat Hill), and include a lamprophyre intrusion (Pilot Knob). Together, these igneous rocks define the Upper Wind River Basin volcanic field (UWRB). All UWRB rocks have large ion lithophile element enrichments, high field strength element depletions, and other geochemical characteristics associated with subduction and that are identical to those of the Miocene Jackson Hole volcanics, even though the former erupted in an intraplate setting. Our results suggest that UWRB magmatism, as well as the Jackson Hole volcanics and other small-volume, similarly aged intermediate to felsic magmatism in eastern Idaho, are the result of the interaction between the North American plate and the progression of the tectonic parabola associated with the Yellowstone hotspot tail.

INTRODUCTION

The identification of volcanism associated with intracontinental hotspots, as well as the hotspot tracks themselves, can be challenging (Courtillot et al., 2003). Hotspot identification is often based on magmatic age progressions, which can be controversial due to errors in geochronology constraints and the issue of linking volcanic events to a specific driving mechanism (Fouch, 2012; Kuehn et al., 2015). Complicating matters, magmatism often continues long after (e.g., millions of years) the upper plate has been translated away from an upwelling plume (Bercovici and Mahoney, 1994; Sleep, 2003; Shervais and Hanan, 2008; Jean et al., 2014). Furthermore, out-of-sequence magmatism assigned to other driving mechanisms—such as "hotlines" due to convection cells in the upper mantle (Meyers et al., 1998), magma overpressurization–induced lithosphere deformation (Hieronymus and Bercovici, 2001), or lateral melt propagation off the hotspot track (Konstantinou et al., 2013)—might overlap with the timing of hotspot magmatism (Kuehn et al., 2015). We propose a new solution to assist in the identification of intracontinental hotspot-related volcanism. This specifically addresses the discrepancy between the ages and occurrence of older "off-track" volcanic products in northwest Wyoming (USA) that are adjacent to a proposed hotspot track yet are out of sequence with the hotspot track age progression.

Nearly all Cenozoic volcanism in Wyoming is associated with the ca. 2.1 Ma to present Yellowstone Plateau volcanic field (Fig. 1) (Christiansen, 2001). However, ~80–100 km southeast of the Yellowstone Plateau volcanic field, coincident with the southern margin of the Absaroka Range in the upper Wind River Basin, Wyoming, are thick packages of Eocene volcanic and volcaniclastic strata related to Farallon plate subduction (Absaroka volcanics; Feeley, 2003). Additionally, <3 Ma alkalic volcanic rocks are found in southwestern Wyoming in the Leucite Hills (Fig. 1; Carmichael, 1967; Lange et al., 2000; Mirnejad and Bell, 2006). Furthermore, in the greater Yellowstone region (northwestern Wyoming, northeastern Idaho, and southwestern Montana), scattered remnants of young (<5 Ma) near-vent deposits, lavas, and intrusives stratigraphically overlie the Eocene strata, generally at high elevations (Fig. 1). Some of these <5 Ma upper Wind River basin rocks were originally mapped by Love (1947), Keefer (1957), and Love et al. (1979) but have remained essentially unstudied by modern techniques until now, and are the focus of this study. Moreover, they appear to be part of a region in northwest Wyoming and northeast Idaho where primarily intermediate-composition rocks with arc-like trace element signatures were either erupted or emplaced during the last ~9 m.y. (Price,

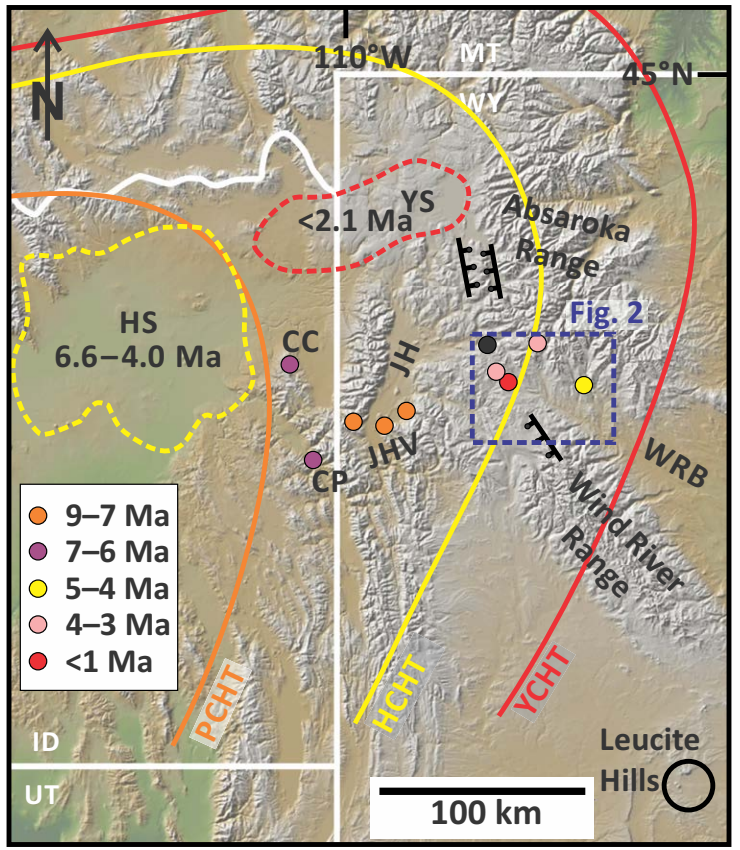

Figure 1. Digital elevation map of northwestern Wyoming (WY), eastern Idaho (ID), and adjacent states (MT—Montana; UT—Utah) (USA) depicting the upper Wind River Basin study area (dashed blue rectangle; Fig. 2), age relations of the Upper Wind River Basin volcanic field (UWRB) and other chemically similar regional rocks related to UWRB magmatism (colored circles: CC—Carlton Creek Volcanics; CP—Palisades Dam–Calamity Point andesite; JHV—Jackson Hole volcanics; black circle is undated Wildcat Hill), location of Snake River Plain–Yellowstone volcanic fields (dashed borders: HS—Heise; YS—Yellowstone; numbers are ages indicating when the volcanic fields were active), the leading edge of the tectonic parabola associated with the Yellowstone Plateau (YCHT—Yellowstone crescent of high terrain), Heise (HCHT—Heise crescent of high terrain), and 10.4–6.6 Ma Picabo (PCHT—Picabo crescent of high terrain) volcanic fields. YCHT location is after Pierce and Morgan (2009), and HCHT and PCHT are inferred. Normal fault zones (black hatched lines; e.g., Upper Yellowstone fault zone, etc.) that extend southeast of Yellowstone Lake and other select geographic features are also depicted: ESRP—eastern Snake River Plain; JH—Jackson Hole; WRB—Wind River Basin. Faults north and south of the study area are from Love et al. (1979) and Christiansen (2001).

2009; Adams, 2014). This includes the ca. 8.5–8 Ma Jackson Hole volcanics, dated by the K-Ar method (Fig. 1; Naeser et al., 1980; Adams, 1997; Lageson et al., 1999), and the ca. 7–6 Ma Carlton Creek Volcanics, dated by the $^{40}Ar/^{39}Ar$ method (Price, 2009). Price (2009) associated the Carlton Creek Volcanics with Basin and Range–related volcanism and noted a compositional similarity to the Jackson Hole volcanics. The proximity of the upper Wind River Basin to the position of the Snake River Plain–Yellowstone hotspot track warrants exploration of any potential relationship between the two.

Prior K-Ar geochronology from three upper Wind River Basin locations yielded ages of ca. 0.48 Ma (Lava Mountain; Rohrer and Obradovich, 1978), ca. 3.4 Ma (Pilot Knob; Rohrer and Obradovich, 1978) and ca. 3.6 Ma (Crescent Mountain; Blackstone 1966) (Figs. 1 and 2). Thus, there is some temporal overlap with the Yellowstone Plateau volcanic field, however the two older ages fall in a gap between Yellowstone volcanism and volcanism related to the Heise volcanic field, which ended at ca. 4 Ma (Morgan and McIntosh, 2005; Ellis et al., 2017).

This study presents field constraints, $^{40}Ar/^{39}Ar$ geochronology, and whole rock geochemistry from three largely unstudied upper Wind River Basin volcanoes (Lava Mountain, Spring Mountain, and Crescent Mountain) and two shallow intrusive bodies (Pilot Knob and Wildcat Hill) (Figs. 1, 2). Aside from the three prior K-Ar ages and two bulk rock geochemical analyses from Crescent Mountain (Blackstone, 1966), the data in this study are the first of their kind from these igneous bodies. The primary purpose of the study is to document the geology of these volcanoes and intrusives. We recognize that the upper Wind River Basin volcanoes and intrusives form a cluster of volcanoes that fits the broad description of a volcanic field as described by de Silva and Lindsay (2015), which we define here as the Upper Wind River Basin volcanic field (UWRB; Fig. 1). This volcanic field, along with the Jackson Hole volcanics and other locally sourced, small-volume eruptive loci in eastern Idaho, are all part of the same group of igneous activity that is not well understood in terms of broader regional tectonic influences such as Basin and Range extension and the Yellowstone hotspot.

GEOLOGICAL BACKGROUND

The UWRB magmatism was influenced by the late Archean Wyoming craton, which stabilized at ca. 2.8 Ga and underlies much of present-day Wyoming, southeastern Montana, and parts of eastern Idaho, western South Dakota, and northern Utah (Mueller and Wooden, 1988; Foster et al., 2006). Craton rocks are now exposed at the surface due to Laramide thick-skinned reverse faulting in many of the regional mountain ranges (e.g., Wind River uplift leading to the Wind River Range and Washakie uplift and Washakie Range which includes Spring Mountain). Wyoming was a stable shelf environment from the Paleozoic to Early Cretaceous, with dominantly marine sedimentation in a shallow epeiric sea environment (Ray and Keefer, 1985). By the Late Cretaceous, marine and non-marine sediments were deposited in the Wind River Basin coinciding with the onset of the Late Cretaceous–early Eocene Laramide orogeny.

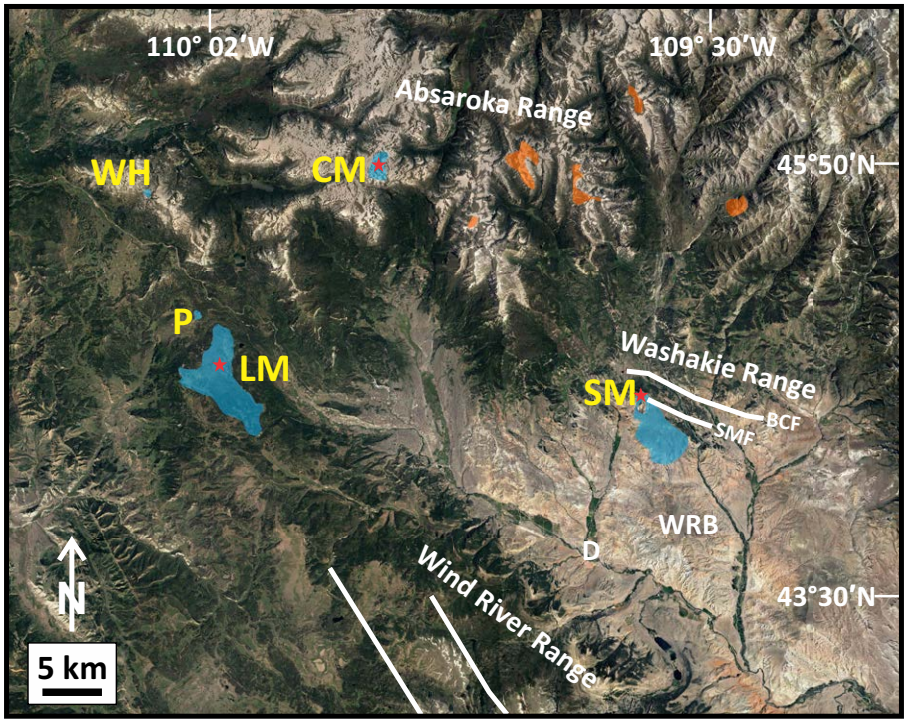

Figure 2. Google Earth satellite image of our study area (dashed rectangle in Fig. 1), northwestern Wyoming (USA). P—Pilot Knob; WH—Wildcat Hill; LM—Lava Mountain; SM—Spring Mountain; CM—Crescent Mountain; WRB—Wind River Basin; D—Dubois, Wyoming. Red stars are identified vent locations. Labeled blue shading shows the extent of studied Upper Wind River Basin volcanic field (UWRB) igneous rocks; orange shading denotes unstudied UWRB volcanics (after Keefer, 1957; Ketner et al., 1966; Love et al., 1979; Protska et al., 1979). White lines indicate normal faults projected from the south from Love et al. (1979) in Wind River Range, and Bear Creek (BCF) and Spring Mountain (SMF) normal faults in the Washakie Range after Keefer (1955) and Winterfeld and Conard (1983). The latter two faults parallel major range-forming Laramide thrust faults (not depicted) of the Washakie uplift.

During the Laramide, mountain ranges developed along high-angle reverse faults and the Wind River Basin began to subside through the early Eocene, resulting in a large sediment influx. Local Laramide structures are evident today in the form of large down-warped anticlines and dome structures in the basin (Ray and Keefer, 1985). By the end of the Eocene, most uplift and subsidence had stopped; however, accumulation of sediment in the Wind River Basin continued through the mid-Miocene (Ray and Keefer, 1985). Precambrian igneous and metamorphic rocks outline the northern, southern, and western flanks of the Wind River Basin (e.g., Wind River uplift to the south and Washakie uplift to the north). These include >10,000 km^3 of late Archean granite, schist, and gneiss cut by mafic dikes (Keefer, 1970). From the Late Cretaceous through early Tertiary, sediments removed during uplift of the Wind River Range were deposited into the central parts of the Wind River Basin until uplift halted in the late Eocene, at ca. 51 Ma (Fan et al., 2011). Pre-Tertiary carbonate and siliciclastic sediments deposited in the basin total ~5 km in thickness (Seeland and Brauch, 1975). Volcaniclastic deposits, including volcanic conglomerate and tuffaceous sandstone, compose much of the Eocene sedimentary strata found in the upper Wind River Basin (Keefer, 1970). In the upper Wind River Basin, these mid-Eocene rocks are dominated by thick (>1 km) packages of lavas, pyroclastics, and volcaniclastic deposits of the Absaroka volcanic field (Keefer, 1970). Local Absaroka volcanism extends from north of Dubois, Wyoming, northwest into Yellowstone and into southwest Montana. The mantle source involved in Absaroka volcanism is thought to be ancient depleted lithospheric mantle that has since been enriched by both older and recent metasomatic events. The latter was most likely associated with the eastward subduction of the Farallon plate under present-day North America (Feeley, 2003).

During the past ~2 m.y., >6000 km^3 of primarily compositionally bimodal felsic and mafic magma has erupted within the Yellowstone Plateau volcanic field (Christiansen, 2001). The most commonly accepted explanation for the origin of the Yellowstone Plateau volcanic field is a stationary mantle plume with shallow manifestations (e.g., seismically imaged magma body) recognized underneath present-day Yellowstone National Park. The origin of the hotspot is still debated, however the volcanism associated with it first occurred along the Idaho-Oregon-Nevada border region, forming the Columbia River–Steens flood basalts between ca. 16.8 and 15.0 Ma (Carlson and Hart, 1987; Camp and Ross, 2004). As the North American plate migrated to the southwest, Yellowstone hotspot-related volcanism migrated to the northeast, eventually forming the eastern Snake River Plain and ultimately the Yellowstone Plateau (Fig. 1).

Recent Yellowstone volcanism includes three major explosive silicic eruptions (cycles one to three) that together helped to form the present-day Yellowstone Plateau volcanic field. The youngest caldera of the Yellowstone Plateau volcanic field was created during the eruption of the 0.64 Ma Lava Creek Tuff (i.e., third cycle). Recent basaltic volcanism that postdates this includes basalts of the Snake River Group, the Osprey Basalt, and the Madison River Basalt (Christiansen et al., 2007). Volumetrically, most Yellowstone Plateau volcanic field extrusive rocks are rhyolite, making up 95% of the entire volcanic field (Christiansen, 1984). The few areas of exposed mafic rocks found within Yellowstone are primarily from the first and third caldera-forming eruptive cycles; basalts followed alternating periods of felsic eruptions in Yellowstone National Park during periods of extension (Christiansen, 2001). Basaltic eruptions after the third cycle of caldera-forming silicic activity are primarily concentrated around areas of previous basaltic volcanism and extensional faulting and are found outside the third-cycle caldera (Christiansen, 2001).

Basin and Range extensional tectonics may have played an important role in the development of UWRB magmatism. In northwest Wyoming, Basin and Range extension is best manifested by large-displacement normal faults and associated half-grabens (e.g., Teton normal fault and Jackson Hole, Wyoming), although numerous other smaller fault systems are present (Machette et al., 2001). Cenozoic normal faults have been mapped in the UWRB, cut Precambrian basement in the Wind River Range, and have also been mapped in the southeast portion of Yellowstone National Park (Figs. 1, 2; Love et al., 1979; Christiansen, 2001). The relationship between Basin and Range extension and the Yellowstone hotspot is debated, but they are likely linked to some degree (Christiansen et al., 2002; Colgan and Henry, 2009; Pierce and Morgan, 2009; Camp et al., 2015). However, regardless of that postulated link, in the greater Yellowstone region, collapse of the Sevier fold-and-thrust belt and Laramide uplifts via normal faulting initiated soon after the end of the Laramide orogeny, well before the ca. 17 Ma inception of the Yellowstone hotspot, and continued into the Miocene (Winterfeld and Conrad, 1983; Steidtmann and Middleton, 1991; Constenius, 1996). Ample evidence exists for regional extensional basin formation by the early to middle Miocene. For example, extension and basin sedimentation occurred just north of Yellowstone National Park in Montana at ca. 18–13 Ma (Barnosky and Labar, 1989; Burbank and Barnosky, 1990), and south in Jackson Hole, Wyoming, and Grand Valley, Idaho, at ca. 16–10 Ma (Barnosky and Labar, 1989; Anders et al., 2009); the latter is associated with the Miocene Jackson Hole volcanics. This Miocene phase of extension has also been linked to Yellowstone plume head–North American plate interaction (Anders et al., 2009), which complicates interpretations as to why it occurred. Subsequent extension in Jackson Hole that continues today, primarily along the Teton normal fault, was initiated at ca. 3 Ma after an ~7 m.y. hiatus (Anders et al., 1989). Mid-Miocene to ongoing extensional processes also affected southwestern Montana and northeastern Idaho, some of which have been linked to the Yellowstone hotspot (Fritz and Sears, 1993; Sears et al., 2009). This extensional tectonic regime continues today along the western side of Wyoming and extends southward past Salt Lake City, Utah, as part of the Intermountain seismic belt and eastern edge of the Basin and Range province (Payne et al., 2012).

The UWRB volcanics and intrusive bodies were initially mapped by Keefer (1957), and subsequent studies by Blackstone (1966), Love et al. (1979), and Protska et al. (1979) provided more detailed field and geochemical constraints on a few of the rocks, though these efforts simply documented their occurrence. One observation that unifies these units is that they all stratigraphically lie above Eocene Absaroka rocks, and in most cases, UWRB lavas lie disconformably on a low-relief erosional surface that developed on the Eocene rocks (Pierce and Morgan, 1992). Lava Mountain was considered Quaternary basalt on the geological map of Yellowstone National Park (Christiansen, 2001) and is a partially dissected shield volcano composed of a pile of at least 26 lava flows capped by a scoria cone (Love and Love, 1983; this study). This study demonstrates that no basalt is present at Lava Mountain, only basaltic andesite to dacite. The prior K-Ar age (0.48 ± 0.06 Ma; Rohrer and Obradovich, 1978) was obtained from a flow near the top of the lava stratigraphy and, if accurate, places Lava Mountain volcanism temporally coincident with the mafic eruptions that followed eruption of the Lava Creek Tuff, forming the third-cycle Yellowstone caldera. K-Ar dating and petrography from Pilot Knob were reported by Rohrer and Obradovich (1978) and Love and Love (1983), who identified the knob as a biotite-augite intrusive (vogesite). Blackstone (1966) mapped Crescent Mountain and described it as an ~150-m-high cinder cone, partially covered by a 60-m-thick package of "basalt" lavas. Two geochemical analyses from Crescent Mountain indicate that the local magmatic products are basaltic andesite to dacite (Blackstone, 1966). Protska et al. (1979) also briefly discussed Crescent Mountain and stated that the lavas are "basaltic" based on geological mapping.

METHODS

Sampling locations were targeted based on published geological maps and satellite imagery. At Lava Mountain, stratigraphic relationships between lavas guided sampling, and the goal was to derive a detailed stratigraphy of the volcanic pile, from its base to the capping scoria cone (Downey, 2015). At Spring Mountain and Pilot Knob, geological mapping accompanied sampling; mapping did not occur at Crescent Mountain or Wildcat Hill. Keefer (1955) mapped highly weathered basaltic lava to the south of Spring Mountain extending down into the upper Wind River Basin north of Dubois; these exposures were unsampled in our study. Only the freshest rocks were targeted for collection and further processing and analysis. Weathered surfaces were removed from samples larger than fist size, which were then split into smaller pieces using a RockLabs hydraulic press. These pieces were powdered using a Spex Industries shatterbox (alumina vessel).

For $^{40}Ar/^{39}Ar$ analysis, two samples were submitted to the Geochronology Laboratory at University of Alaska Fairbanks (UAF; Alaska, USA) where they were crushed, sieved, washed, and hand-picked for phenocryst-free whole-rock

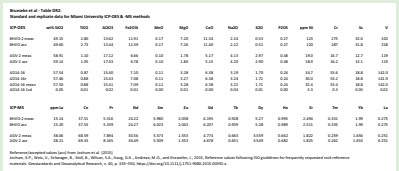

[1]Supplemental Tables. Table S1: Detailed step heat data for $^{40}Ar/^{39}Ar$ geochronology. Table S2: Standard and replicate data for Miami University ICP-OES and -MS methods. Table S3: Major and trace element geochemistry. Please visit http://doi.org/10.1130/GES01553.S1 or the full-text article on www.gsapubs.org to view Table S1.

groundmass chips. The monitor mineral TCR-2 (sanidine from the Taylor Creek Rhyolite; Duffield and Dalrymple, 1990) with an age of 28.619 Ma (Renne et al., 2010) was used to monitor neutron flux and calculate the irradiation parameter (*J*) for all samples. The samples and standards were wrapped in aluminum foil and loaded into aluminum cans of 2.5 cm diameter and 6 cm height. The samples were irradiated in position 8c of the enriched-uranium research reactor of McMaster University (Ontario, Canada) for 20 MWh. Upon their return from the reactor, the samples and monitors were loaded into 2-mm-diameter holes in a copper tray that was then loaded in an ultrahigh-vacuum extraction line. The monitors were fused, and samples heated, using a 6 W argon-ion laser following the technique described in York et al. (1981), Layer et al. (1987), and Benowitz et al. (2014). Argon purification was achieved using a liquid nitrogen cold trap and a SAES Zr-Al getter at 400 °C. The samples were analyzed in a VG-3600 mass spectrometer at the Geophysical Institute, UAF. The argon isotopes measured were corrected for system blank and mass discrimination, as well as calcium, potassium, and chlorine interference reactions following procedures outlined in McDougall and Harrison (1999). Typical full-system eight-minute laser blank values were generally 2×10^{-16} mol ^{40}Ar, 3×10^{-18} mol ^{39}Ar, 9×10^{-18} mol ^{38}Ar, and 2×10^{-18} mol ^{36}Ar, which are 10–50 times smaller than the similar sample and standard molar gas releases. Correction factors for nucleogenic interferences during irradiation were determined from irradiated CaF_2 and K_2SO_4 as follows: $(^{39}Ar/^{37}Ar)Ca$ ($^{39}Ar/^{37}Ar$ produced from Ca in the nuclear reactor) = 7.06×10^{-4}, $(^{36}Ar/^{37}Ar)Ca = 2.79 \times 10^{-4}$ and $(^{40}Ar/^{39}Ar)K = 0.0297$. Mass discrimination was monitored by running calibrated air shots. The mass discrimination during these experiments was 0.8% per mass unit. While doing our experiments, calibration measurements were made on a weekly and monthly basis to check for changes in mass discrimination, with no significant variation observed during these intervals. A summary of both of the $^{40}Ar/^{39}Ar$ results is given in Table 1, with all ages quoted to the ±1σ level and calculated using the constants of Renne et al. (2010). We did not take into account the error on the decay constant nor the error on the age of the flux monitor in our calculations, which withstanding the effects on overall error would be small given their limited contribution to overall uncertainty. Detailed step heat data are provided in Supplemental Table S1[1]. The integrated age is the age given by the total gas measured and is equivalent to a potassium-argon (K-Ar) age. The spectrum provides a plateau age if three or more consecutive gas fractions represent at least 50% of the total gas release and are within two standard deviations of each other (mean square weighted deviation <2.5).

Inductively coupled plasma–optical emission spectrometry (Agilent 720ES ICP-OES) analyses of seventeen samples (AD14 and ZD14 series) were completed at Miami University (Ohio, USA) following the methods outlined by Katoh et al. (2016). This included major (Si, Al, Ti, Fe, Mn, Mg, Ca, Na, K, and P) and trace (Ni, Cr, Sc, V, Ba, Rb, Sr, Zr, Nb, Cu, Co, Zn, Pb, Y) element analyses. Table S2 [footnote 1] provides the results for standard reference materials BHVO-2 and AGV-2 run with the AD14 and ZD14 series samples and for multiple analyses of sample AD14-16. Five MB13 series samples were analyzed for major and trace element chemistry via a Panalytical PW 4204 X-ray fluorescence (XRF) spectrometer at Franklin and Marshall College (Pennsylvania, USA), following the methods outlined in Mertzman (2000, 2015) and online at http://www.fandm.edu/earth-environment/laboratory-facilities/.

A full rare earth element (REE) suite—La, Ce, Pr, Nd, Sm, Eu, Gd, Tb, Dy, Ho, Er, Tm, Yb, and Lu—was determined for selected AD14, ZD14, and MB13 series samples at Miami University by inductively coupled plasma–mass spectrometry (ICP-MS). Initial solutions for unknowns and reference materials BHVO-2 and AGV-2 (Table S2 [footnote 1]) were generated via flux fusion involving the following steps: (1) 200 mg of dried powder was combined with 600 mg lithium metaborate ($LiBO_2$) in a pre-fired graphite crucible and fused at 950 °C for 20 min, and (2) after cooling, the resulting glass beads were added to 80 mL of 5% high-purity HNO_3 and agitated on a gyratory shaker until total dissolution was achieved. A zero standard (processing blank) was prepared following the same steps using only 200 mg of $LiBO_2$. The REEs were quantitatively isolated from these solutions through cation exchange chromatography using Dowex 50W-X12 resin, and the REE fractions were eluted with 40 mL of 5N HNO_3. After drying on a hotplate, the REE fractions were brought back into solution in 20 mL of 0.3N HNO_3. These final solutions were analyzed in a Varian 820 ICP-MS equipped with an autosampler. The blank and a set of four synthetic REE standard solutions were used for calibration and were analyzed at the beginning of the instrument session. Background adjusted counts were corrected for within-run drift through the use of mass-appropriate internal standards (^{115}In and ^{185}Re).

TABLE 1. SUMMARY OF NEW $^{40}Ar/^{39}Ar$ AGE RESULTS

Sample	Whole rock	Integrated age (ka)	Plateau age (ka)	Plateau information	Isochron age (ka)	Isochron or other information
MB13-3	Spring Mountain basalt	4791 ± 150	**4791 ± 150**	12 out of 12 fractions 100.0% ^{39}Ar release MSWD = 0.3	4841 ± 337	12 out of 12 fractions $^{40}Ar/^{36}Ar_i$ = 295.4 ± 3.1 MSWD = 0.32
AD14-17	Lava Mountain basaltic andesite	549 ± 145	**397 ± 48**	5 out of 9 fractions 66.5% ^{39}Ar release MSWD = 0.82	426 ± 88	5 out of 9 fractions $^{40}Ar/^{36}Ar_i$ = 294.0 ± 3.9 MSWD = 1.04

Note: Samples were analyzed with standard TCR-2 (age: 28.619 Ma). Most robust age is in bold. MSWD—mean square weighted deviation; $_i$—sample initial $^{40}Ar/^{36}Ar$.

We collected LMT and CRM series samples, and these were processed and analyzed for major and trace elements and REEs via XRF and ICP-MS at Washington State University (Washington, USA) using a ThermoARL Advant'XP+ sequential XRF spectrometer and an Agilent 7700 ICP-MS (REEs) following the methods of Johnson et al. (1999) and Gaschnig et al. (2011).

Twenty-five Lava Mountain, five Spring Mountain, six Pilot Knob, two Wildcat Hill, and six Crescent Mountain samples were analyzed for bulk rock geochemistry. Total volatile loss on ignition was determined for AD, ZD, and MB series samples and is reported with representative major and trace element results in Table 2 (and also in Table S3 [footnote 1]). Iron was split into Fe^{+2} and Fe^{+3} according to the procedure described by Le Maitre (1976), and all major element data used in diagrams and the discussion are reported as anhydrous using the split iron data.

RESULTS

Field Relationships, Physical Characteristics, and Geochronology

The geochemistry of UWRB magmas will be discussed in detail below; however, to establish a common nomenclature and describe their petrography, initial classification has been made via a total alkalies–versus–silica diagram (Le Bas et al., 1986) (Fig. 3). Lava Mountain rocks plot as basaltic andesites, andesites, and dacites, and Spring Mountain rocks are basalts. Crescent Mountain samples are basaltic andesites and dacites, while Pilot Knob samples plot as basaltic trachyandesites and Wildcat Hill rocks are andesite to dacite.

Based on its shape and areal extent, Lava Mountain is a shield volcano and the volume of erupted material is ~5.5 km^3 (Downey, 2015). Lava Mountain shows evidence of being affected by post-volcanic glaciation, including truncated cliffs that expose the lavas (Figs. 4A, 4B). Field observations and geochemistry indicate that there are stratigraphic variations in magma composition; i.e., the basal ~100 m of the volcano was dominated by broadly mafic and felsic eruptions (basaltic andesite and dacite; Fig. 3), while the upper 400 m, including the capping cone, is andesitic. The youngest and stratigraphically highest unit on Lava Mountain is a scoria cone composed of slightly oxidized andesite scoria and bombs, located on the eastern side of the mountain (Figs. 4A, 4C). Andesite lavas that crop out stratigraphically lower than the scoria cone exhibit both platy and blocky characteristics in cross-section (Figs. 4B, 4D). Most andesite lavas are platy and exhibit sheet jointing in those units immediately above a basal breccia consisting of scoriaceous clasts. Individual platy lavas range from 10 to 50 m thick. Most are not horizontal throughout their lateral extent, but tend to ramp and curve due to flow (Fig. 4D). Elongated vesicles ~3 cm and smaller in maximum dimension are common in these lavas. Outcrops of blocky basaltic andesite lavas range up to 15 m high and are commonly autobrecciated (Fig. 4E). Dacite lavas occur near the base of Lava Mountain and are characterized by upper and lower vitrophyres.

The basaltic andesites from Lava Mountain are aphanitic with sparse phenocrysts of 0.25–2 mm orthopyroxene and are commonly vesicular. Two groups of basaltic andesites were observed. One consists of light tan to gray rocks that show light banding and contain ~5% orthopyroxene phenocrysts. Rocks of the other group are blocky and contain more phenocrysts but fewer vesicles. The orthopyroxenes are subhedral to anhedral, and many are resorbed. The major distinguishing petrographic feature separating the basaltic andesites from other Lava Mountain volcanics is the presence of olivine phenocrysts in all samples (Fig. 5A). Although not very abundant (~3%–7% modally), the olivines are euhedral to anhedral and average 0.3–0.6 mm in size; some exhibit skeletal morphologies. Groundmass ranges from 75% to 90% of the rocks and consists of plagioclase, orthopyroxene, and Fe-Ti oxides. A single 4.6 mm quartz xenocryst is also present in one sample. The andesites generally have an aphanitic groundmass (~65%–98%) with pyroxene phenocrysts (up to 3 mm). All contain vesicles (elongated up to 3–5 cm) and have ~6%–24% orthopyroxene phenocrysts modally; none contain olivine. Orthopyroxene is typically euhedral to subhedral and includes slightly resorbed and zoned crystals. Rounded and complexly zoned plagioclase (2–6 mm) is also present, as well as orthopyroxene with complex reaction rims. Major xenocrysts include an anhedral and partially resorbed alkali feldspar and plagioclase crystals with reaction rims. The most silica-rich samples collected at Lava Mountain are the dacites, which are dominated by groundmass; collected samples are vitrophyric (~96%–97% groundmass) and are black and glassy in hand sample. Trachytic texture is apparent in the groundmass, and most of these plagioclase crystals have a swallowtail texture. Some 0.4–0.6 mm plagioclase crystals are also rounded and resorbed (Fig. 5B) (<2% modally), and one 1.8 mm clinopyroxene was also observed, as well as trace apatite microlites.

Pilot Knob is ~2 km west of Lava Mountain (Figs. 2, 4F) and was emplaced through Eocene sedimentary strata (Dodd, 2015). The intrusion is rounded, but tapers to a southeast-trending ridge-like "fin" at the summit, which we interpret to possibly reflect the base of a dike (Fig. 4F). Glacier erosion–formed boulder fields made of the Pilot Knob intrusive rocks surround in situ bedrock (Figs. 4F, 4G). All Pilot Knob samples we collected are coarse to medium grained and average ~67.1% plagioclase, 14.5% clinopyroxene, 6.5% phlogopite, 6% orthopyroxene, and 6% apatite (Fig. 5C). Although plagioclase is the dominant mineral phase, it occurs primarily in the groundmass, where it is fine grained (<0.25 mm), is euhedral to subhedral, and exhibits strong Carlsbad twinning. Some plagioclase phenocrysts were also noted. Apatite crystals are commonly poikilitically enclosed within the plagioclase. Clinopyroxene crystals range from 0.5 to 1.5 mm in size; they typically exhibit sieve and resorption textures and were noted in both phenocryst and groundmass occurrences. The poikilitic orthopyroxenes present do not appear as weathered as the clinopyroxene and are intergrown with plagioclase crystals as glomerocrysts. Phlogopites are 2–25 mm in size throughout all Pilot Knob samples and commonly appear altered along the outer rims (Fig. 5C). Trace amounts of zircon were also noted in the groundmass. Pilot Knob rocks identified in this study are classified as lamprophyre (Rock, 1977; Woolley et al., 1996). Many

TABLE 2. REPRESENTATIVE GEOCHEMICAL ANALYSES OF UPPER WIND RIVER BASIN IGNEOUS ROCKS

Sample	MB13-3	MB13-4B	AD14-17	AD14-9	AD14-10	AD14-4	ZD14-2	ZD14-19A	CRM2	CRM4
Location / sample type	Spring Mtn. lava	Spring Mtn. lava	Lava Mtn. lava	Lava Mtn. lava	Lava Mtn. lava	Lava Mtn. scoria	Pilot Knob intrusion	Wildcat Hill intrusion	Crescent Mtn. lava	Crescent Mtn. dike
SiO_2	50.23	50.01	55.29	57.94	62.35	58.06	54.08	63.08	66.09	52.29
TiO_2	0.71	0.92	0.84	0.88	0.89	0.79	0.87	0.69	0.62	0.90
Al_2O_3	14.44	16.69	15.60	15.91	15.97	15.60	16.50	15.95	15.58	14.48
Fe_2O_3	9.75	9.79	7.99	7.66	6.74	7.24	6.27	5.23	4.58	7.77
MnO	0.15	0.15	0.12	0.12	0.10	0.11	0.09	0.07	0.06	0.11
MgO	11.41	7.68	6.49	4.72	2.27	5.20	5.61	3.06	2.42	8.96
CaO	10.37	11.30	8.04	7.25	5.64	7.10	7.80	5.07	4.01	8.95
Na_2O	2.01	2.26	2.74	3.07	3.33	2.95	2.95	3.54	3.45	2.41
K_2O	0.58	0.61	1.65	1.72	1.69	1.91	3.66	2.27	2.80	2.64
P_2O_5	0.17	0.20	0.28	0.27	0.21	0.26	0.60	0.20	0.17	0.52
LOI	1.19	1.26	0.02	–0.13	–0.01	0.16	0.33	0.45	N.D.	N.D.
Total	100.26	100.04	99.05	99.53	99.19	99.22	98.42	99.16	99.32	98.22
Ni	295	95	115	69	11	87	117	63	45	259
Cr	955	255	271	126	27	215	142	88	81	500
Sc	28	30	25	22	16	21	15	11	9.9	20
V	210	231	169	160	127	146	127	86	80	127
Ba	544	458	1563	1520	1141	1481	2690	1274	1129	2196
Rb	10	11	22	22	21	33	45	43	73	38
Sr	430	490	666	759	600	633	2147	606	392	1748
Zr	95	105	155	166	176	178	285	167	214	238
Nb	4.2	5.1	19	17	8.7	15	7.9	9.4	10	13
Cu	66	31	32	42	22	34	34	28	16	45
Co	58	46	33	29	18	28	28	16	N.D.	N.D.
Zn	75	76	77	79	88	77	73	66	71	79
Pb	14	<1	10	12	14	15	33	19	21	25
La	24.1	31.8	52.4	56.7	44.8	57.7	169	53.5	53.1	140
Ce	47.1	61.6	101	109	88.6	112	339	102	103	277
Pr	5.28	6.67	11.1	12.1	10.0	12.4	39.6	11.2	11.4	31.8
Nd	19.3	24.4	40.4	44.0	37.9	45.3	143	41.0	41.1	114
Sm	3.51	4.21	6.37	6.81	6.47	7.31	19.4	6.59	7.31	16.0
Eu	1.02	1.24	1.63	1.76	1.77	1.72	4.24	1.59	1.45	3.58
Gd	3.21	3.99	5.31	5.64	5.62	6.06	9.60	5.30	5.40	8.77
Tb	0.52	0.62	0.74	0.78	0.80	0.83	1.02	0.70	0.78	1.01
Dy	3.11	3.68	4.14	4.32	4.53	4.60	4.69	3.63	4.33	4.93
Ho	0.65	0.77	0.82	0.85	0.89	0.90	0.81	0.69	0.79	0.88
Er	1.79	2.11	2.31	2.39	2.51	2.53	1.97	1.84	2.07	2.19
Tm	0.26	0.31	0.33	0.34	0.36	0.36	0.27	0.26	0.28	0.31
Yb	1.70	2.00	2.22	2.25	2.37	2.36	1.60	1.68	1.72	1.81
Lu	0.25	0.30	0.33	0.33	0.35	0.35	0.24	0.25	0.26	0.28

Note: All major element data expressed as raw weight percent (wt%) oxides; all other concentrations in parts per million (ppm). Mtn.—Mountain; LOI—loss on ignition; N.D.—not determined.

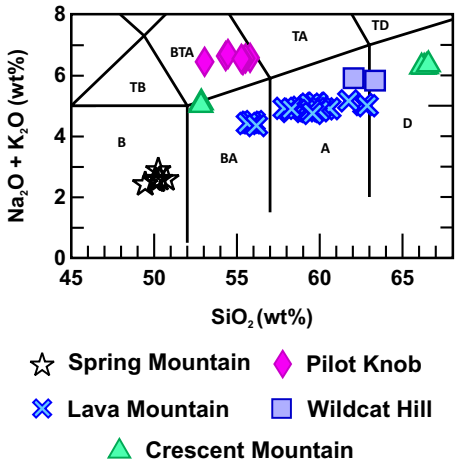

Figure 3. Classification of studied volcanic rocks based on total alkalies versus silica (Le Bas et al., 1986). B—basalt; BA—basaltic andesite; A—andesite; D—dacite; TB—trachybasalt; BTA—basaltic trachyandesite; TA—trachyandesite; TD—trachydacite.

lamprophyres plot within the field of trachybasalt on a total alkalis–versus–silica diagram (Le Bas and Streckeisen, 1991), but this geochemical classification overlooks some of the distinctive petrographic features of lamprophyres. For this reason, lamprophyres are commonly classified based on their mineralogy rather than their geochemistry. We classify Pilot Knob as a lamprophyre based on modal mineralogy because it fits the lamprophyre characteristics outlined by Le Maitre et al. (2002). This classification is consistent with its bulk chemical composition. The hydrous mineral phase in Pilot Knob is exclusively mica, and its mineralogical composition is primarily phlogopite (Dodd, 2015). Therefore, the Pilot Knob intrusion is a kersantite lamprophyre (Le Maitre et al., 2002).

Wildcat Hill is exposed ~5 km northwest of Pilot Knob and occurs along an apparent fault zone on strike with a major regional normal fault zone that is mapped ~10 km northwest of Pilot Knob (Fig. 1; Christiansen, 2001). Wildcat Hill also intrudes Eocene rocks (e.g., Absaroka volcanics and volcaniclastic strata) (Fig. 4H). Well-developed columnar jointing and two different petrographic types characterize the intrusion: a glassy outer margin of the intrusion (sample ZD14-19b) and a vesiculated (in places), blocky interior (ZD14-19a). The Wildcat Hill intrusion is hypabyssal in origin, with more fine-grained textures than Pilot Knob. Both samples from Wildcat Hill (ZD14-19a and ZD14-19b) appear homogenous in composition, with ~72.4% groundmass, 8.8% clinopyroxene, 8.5% plagioclase, 7.5% biotite, and 3.2% orthopyroxene (Fig. 5D). A plagioclase-dominated matrix within Wildcat Hill consists of primarily <0.1 mm plagioclase crystals with some plagioclase phenocrysts up to 0.3 mm in length. Pyroxene crystals are ~0.5 mm.

At Spring Mountain, ~38 km east of Lava Mountain, basalts erupted along high-angle normal faults that cut Paleozoic and Eocene strata (1:24,000-scale field mapping by C. Haley, W. Hart, and M. Brueseke (1999–2000); Figs. 1, 2, 4I). These faults are likely part of a more extensive southeast-trending fault system mapped by Keefer (1955) that extends southeast of Spring Mountain (Spring Mountain fault; Fig. 2). Keefer (1955, 1957) showed that erupted lavas flowed south into the upper Wind River Basin. Based on our observations, Spring Mountain volcanism is likely the result of one monogenetic event. Eruptions were focused along faults and were fissure eruptions; large amounts of pervasively oxidized scoria mark the vents (Figs. 4I, 4J, 4K). Textural variation exists among the Spring Mountain basalt and three different textural varieties are present: fine-grained, coarse-grained, and scoria (Fig. 4J). Coarse-grained samples contain ~0.25–0.5 mm olivine phenocrysts and are vesicular. The fine-grained variety (sample MB13-4B) has an aphanitic, non-vesiculated groundmass, but does have fresh iridescent olivine phenocrysts (average ~0.5 mm). In thin section, Spring Mountain basalts are primarily holocrystalline, with subhedral to euhedral olivine phenocrysts and glomeroporphyritic clusters in a fine-grained groundmass (Fig. 5E). Olivine occurs as a phenocryst and groundmass phase in all samples. The phenocrysts can be euhedral, resorbed, and/or skeletal, occasionally with iddingsite rims. Groundmass plagioclase is ubiquitous and has a trachytic texture. Ophitic and subophitic textures are also common in all samples, with plagioclase intergrown with clinopyroxene and olivine. Clinopyroxenes in these rocks are smaller than olivine crystals, averaging only ~0.1 mm in size.

The Crescent Mountain volcano was not mapped in detail as part of this study, but was sampled. Blackstone (1966) mapped a partially dissected scoria cone, as well as a local intrusive dike and package of lavas, all stratigraphically overlying and/or cutting Eocene deposits (Fig. 4L). The cone is estimated to be ~5 km^2 in extent, and the lava package is interpreted to have erupted after cone formation; both were intruded by the dike (Blackstone, 1966). It appears to be a monogenetic volcano. New sampling and geochemistry indicate that the two geochemical analyses published by Blackstone (1966) were switched; his "andesitic basalt" unit Tpb (samples CRM1, CRM2, CRM3, CRM5) is in fact dacite lavas, while trachyandesite unit Tpi (samples CRM4, CRM4a) is a basaltic andesite dike. Crescent Mountain dacite lavas have abundant sheet jointing and are aphanitic, with ~20%–25% 1–2 mm phenocrysts of plagioclase, clinopyroxene, and rare olivine (Blackstone, 1966; Fig. 5F). Blackstone's unit Tpi, which crosscuts the cone and lava package, is more crystal rich, with ~30%–35% phenocrysts of 1–2 mm pyroxene and olivine, and <1 mm plagioclase, in a fine-grained trachytic to pilotaxitic matrix (Blackstone, 1966). Blackstone (1966) also reported mica and alkali feldspar in this unit, however we could not substantiate this occurrence.

As discussed above, two UWRB samples—AD14-17 (basal basaltic andesite lava at Lava Mountain) and MB13-3 (Spring Mountain basalt)—were successfully dated to augment existing K-Ar ages from UWRB rocks (Fig. 6; Table 1; Table S1 [footnote 1]). We made multiple attempts to date the capping andesite scoria (AD14-4) at Lava Mountain, but limited radiogenic ^{40}Ar (integrated ~0.04%) precluded an interpretable age, indicating a possible young age (<ca. 400 ka) for this eruptive event (Table S1 [footnote 1]). A homogeneous, phenocryst-free whole rock separate from sample AD14-17 (integrated ~2.1% radiogenic ^{40}Ar) was analyzed. The integrated age (549 ± 145 ka) and the plateau age (397 ± 48 ka) and isochron age (426 ± 88 ka) are all within error of each other.

Figure 4 (*on this and following page*). (A) View of Lava Mountain looking northwest from along the Wind River. Summit scoria cone is present at the left of the image, and glacially truncated cliffs along the right side are ~300 m high. (B) Closeup of Lava Mountain stratigraphy in the glacially carved cliff shown in A, illustrating numerous stacked intermediate-composition lavas. Trees are ~20 m tall. (C) Andesite scoria and bombs on top of Lava Mountain; sample AD14-4. (D) Andesite lava from Lava Mountain, ~3–5 m thick; sample AD14-9. Oxidized basal autobreccia (denoted by arrow) grades into platy, stony lava above, and individual plates are 2–10 cm thick. (E) Blocky, vesicular basaltic andesite at the northwest base of Lava Mountain; sample AD14-18. Rock hammer is 40 cm long. (F) Northwest view of Pilot Knob from the northern flank of Lava Mountain. Eocene Wiggins Formation (Absaroka volcanics) in the background.

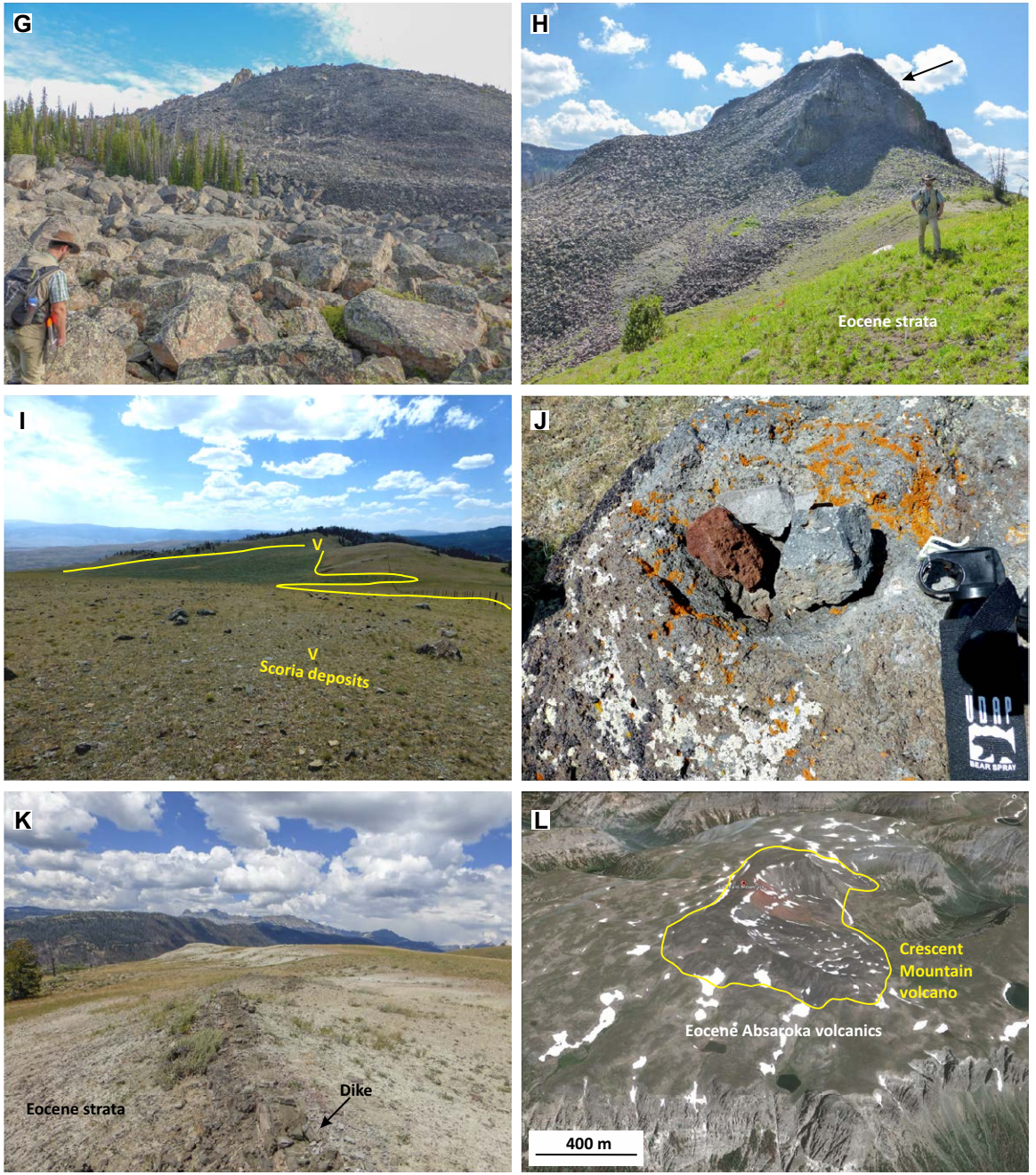

Figure 4 (*continued*). (G) Southwest side of Pilot Knob, with a glacier-derived boulder field. Person is ~1.8 m tall. (H) Southwest view of Wildcat Hill showing the intrusion (cliffs indicated with black arrow) cutting through Eocene strata. (I) Spring Mountain basalt vents (labeled with V) and lava extent. Vent area in distance is MB13-3 sample location. Pervasively oxidized spatter is found in the foreground, partially defining one fissural vent. The lava forms a constructional feature in the valley in center of the image; surrounding rocks in the low hills (~3–4 m high) are Paleozoic sedimentary strata. (J) Megascopic variations in basalt at Spring Mountain. Oxidized scoria to the left, coarse-grained basalt to the right (sample MB13-4A), and fine-grained basalt at the top (sample MB13-4B), on top of a vesiculated basalt boulder. Bear spray canister is 21.6 cm long and 5 cm wide. (K) ~1-m-wide dike (denoted by arrow) cutting through Eocene strata just north of Spring Mountain; this dike petrographically resembles Upper Wind River Basin volcanic field intermediate rocks. (L) Google Earth satellite image of Crescent Mountain, illustrating the scoria cone and surrounding lavas that erupted on a low-relief surface of Eocene Absaroka volcanics.

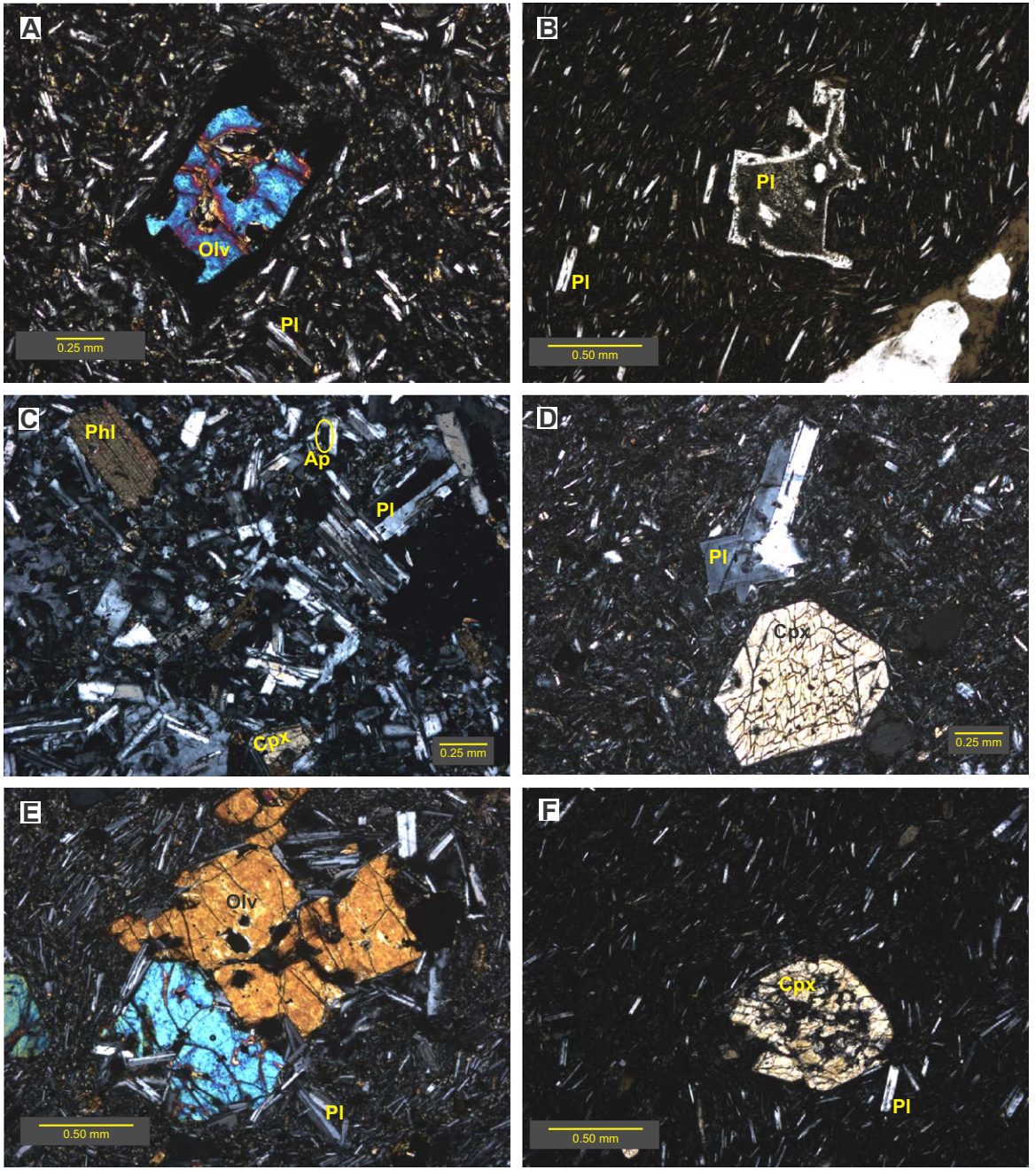

Figure 5. Photomicrographs of representative Upper Wind River Basin volcanic field samples (all cross-polarized light at 4× magnification) Olv—olivine; Pl—plagioclase; Ap—apatite; Phl—phlogopite; Cpx—clinopyroxene. (A) Sample AD14-17; Lava Mountain basaltic andesite. Skeletal olivine with oxide rim surrounded by plagioclase + oxide–dominated matrix. (B) Sample AD14-12; Lava Mountain dacite. Anhedral and resorbed plagioclase surrounded by plagioclase + oxide vitrophyric matrix. (C) Sample ZD14-2; Pilot Knob. Note phlogopite phenocrysts (large phlogopite in upper left) surrounded by smaller plagioclase, pyroxene, oxides, and apatite crystals. (D) Sample ZD14-19a; Wildcat Hill. Clinopyroxene and plagioclase phenocrysts in plagioclase + oxide–dominated matrix. (E) Sample MB13-3; Spring Mountain basalt. Note large olivine phenocrysts, surrounded by smaller plagioclase laths in matrix. (F) Sample CRM2; Crescent Mountain dacite. Resorbed clinopyroxene phenocryst in plagioclase + oxide–rich glassy matrix.

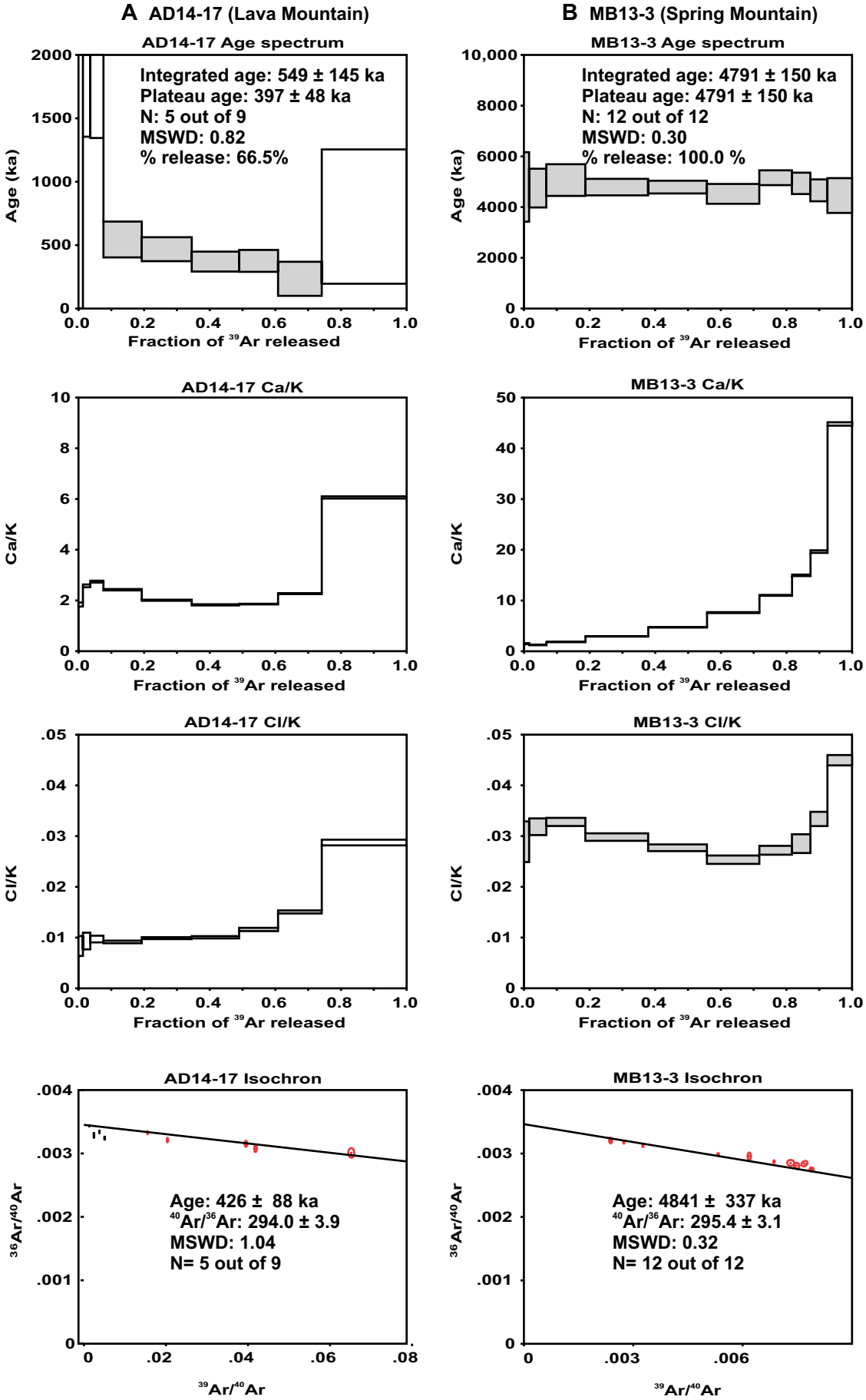

Figure 6. $^{40}Ar/^{39}Ar$ age spectra, Ca/K and Cl/K ratios, and isochrons for the newly dated samples. Steps filled in gray were used for plateau age determinations. Red data points were used for isochron age determinations. N—number of steps and/or data points used for age determinations. MSWD—mean square weighted deviation.

We prefer the plateau age of 397 ± 48 ka for sample AD14-17 because of the higher precision over the isochron age determination. A homogeneous, phenocryst-free whole rock separate from sample MB13-3 (integrated ~12.0% radiogenic ^{40}Ar) was analyzed. The isochron regression to $^{40}Ar/^{36}Ar_i$ ($_i$ is sample initial $^{40}Ar/^{36}Ar$) indicates no evidence of excess ^{40}Ar. The integrated age (4791 ± 150 ka) and the plateau age (4791 ± 150 ka) and isochron age (4841 ± 337 ka) are all within error of each other. We prefer the plateau age of 4791 ± 150 ka for sample MB13-3 because of the higher precision over the isochron age determination.

Geochemical Classification and Bulk Rock Geochemistry

We report new major and trace element bulk chemistry for 44 samples. Major elements are reported as weight percent (wt%) oxide, and trace elements as parts per million (ppm). Table 2 illustrates representative samples, with the full data set in Table S3 [footnote 1]). As discussed earlier, UWRB samples plot either as basalts, basaltic andesites, basaltic trachyandesites, andesites, or dacites (Fig. 3). They also exhibit two distinct suites: a subalkaline suite defined by Spring Mountain basalts, Lava Mountain, Wildcat Hill, and dacite lavas of Crescent Mountain, and a transitional to alkaline suite, defined by the Crescent Mountain basaltic andesite dike and Pilot Knob (Fig. 3). On an alkali-FeO*-MgO (AFM, where FeO* is total Fe expressed as FeO) diagram, only Spring Mountain basalts are tholeiitic (olivine tholeiites based on normative mineralogy); all of the rest are clearly calc-alkaline (Fig. 7). Major and trace element variations of rocks from each volcano or intrusive are plotted in Figures 8, 9, and 10. While broadly similar, it is apparent that samples from each location are chemically distinct from each other. Lava Mountain samples range from 55.5 to 62.8 wt% SiO_2, and MgO, CaO, FeO*, CaO, and P_2O_5 all

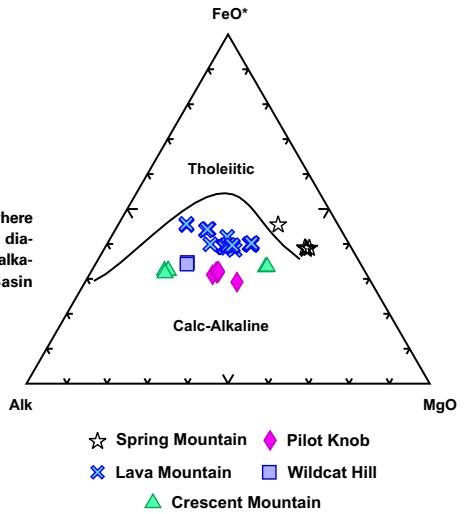

Figure 7. Alkali-FeO*-MgO (AFM, where FeO* is total Fe expressed as FeO) diagram illustrating the primarily calc-alkaline nature of Upper Wind River Basin volcanic field rocks.

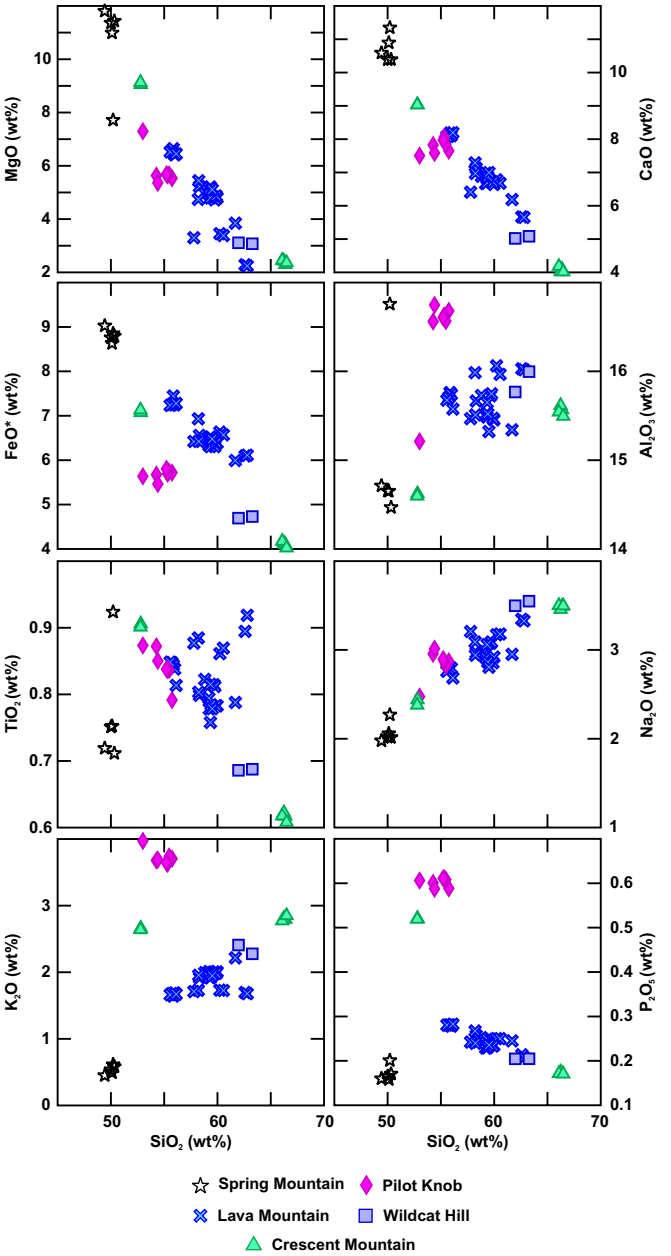

Figure 8. Harker diagrams illustrating representative major element variations of Upper Wind River Basin volcanic field rocks.

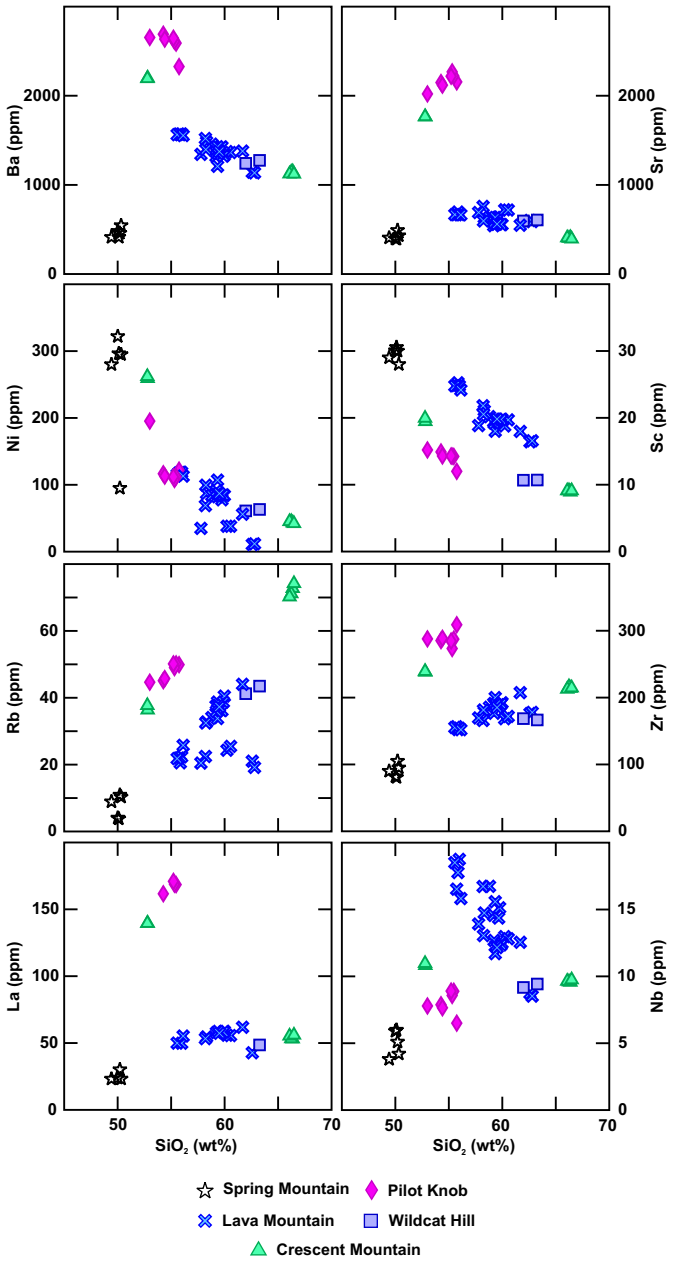

Figure 9. Harker diagrams illustrating representative trace element variations of Upper Wind River Basin volcanic field rocks.

decrease with increasing SiO_2 while Na_2O and K_2O increase (Fig. 8). Spring Mountain basalts average ~50 wt% SiO_2, and major elements show no obvious relationship with SiO_2, though one sample has higher TiO_2 and Al_2O_3 and lower MgO than the rest (Fig. 8). Pilot Knob samples have lower FeO*, MgO, and CaO and higher Al_2O_3, Na_2O, K_2O, and P_2O_5 at a given weight percent SiO_2 than Lava Mountain rocks (Fig. 8). Pilot Knob K_2O values range from 3.6 to 4.0 wt%, which is much higher than in any other UWRB sample. A similar relationship is exhibited by the Crescent Mountain dike (e.g., high K_2O, P_2O_5), but at the highest SiO_2 values, Crescent Mountain lavas fall along the co-linear array of increasing or decreasing major elements versus SiO_2 defined by Lava Mountain (Fig. 8). Wildcat Hill samples also fall along this array at slightly higher SiO_2 than Lava Mountain (Fig. 8). Trace element contents of UWRB samples show variations akin to those of the major elements; however, the differences between locations are more clearly depicted. This provides further evidence that each of these eruptive loci and intrusions represents a separate magmatic system (Fig. 9). Pilot Knob is characterized by high Ba (>2000 ppm), Sr (>1700 ppm), Zr (>200 ppm), Rb (>30 ppm), and La (>160 ppm); only the Crescent Mountain dike has similar trace element characteristics (Fig. 9). These incompatible element abundances are significantly higher than in any other unit, and clear differences are also present in other trace elements (e.g., Nb, Sc) that show lower concentrations at the same SiO_2 value. Sampled Spring Mountain basalts have nearly identical trace element signatures to each other, generally forming a tight cluster on Harker diagrams, except for Ni and Cr (Cr not shown in Fig. 9), which is accounted for by differences in modal olivine (Fig. 9). Lava Mountain basaltic andesites, andesites, and dacites are also distinguishable from other units on these diagrams. Lava Mountain dacites have the lowest overall Ni (<12 ppm) and Cr (<27 ppm) concentrations, which contrasts strongly with the basaltic andesites carrying Ni concentrations >115 ppm and Cr concentrations >240 ppm. Overall, compatible elements Cr, V, Co, Sc, and Ni all decrease with silica (Co, V not shown in Fig. 9). Positive correlations are observed between Sc, Ni, and Cr, suggesting pyroxene fractionation.

A suite of representative samples from each location illustrates the same enrichments and depletions on a primitive mantle–normalized multi-element diagram (Fig. 10). All have pronounced large ion lithophile element (LILE) enrichment and high field strength element (HFSE) depletion. This is characteristic of subduction zones (Fig. 10). The Spring Mountain basalts are generally enriched in all elements except for Ti and REEs relative to normal mid-ocean-ridge basalt (N-MORB) and are clearly distinct from ocean-island basalt (OIB) (Fig. 10). These enrichments and observed relative depletions are reminiscent of basalts derived from lithospheric mantle enriched by prior subduction processes (Kempton et al., 1991). All of the UWRB rocks have steep light REE (LREE) patterns. The Pilot Knob and Crescent Mountain samples exhibit the highest degree of LREE enrichment and flat to slightly curved downward heavy REE (HREE) patterns relative to chondrite (Fig. 11). All Lava Mountain REEs show a small increase in concentration against SiO_2, which is consistent with fractional crystallization of phases that exclude REEs, and small negative Eu anomalies due to plagioclase crystallization. Such LREE enrichment and

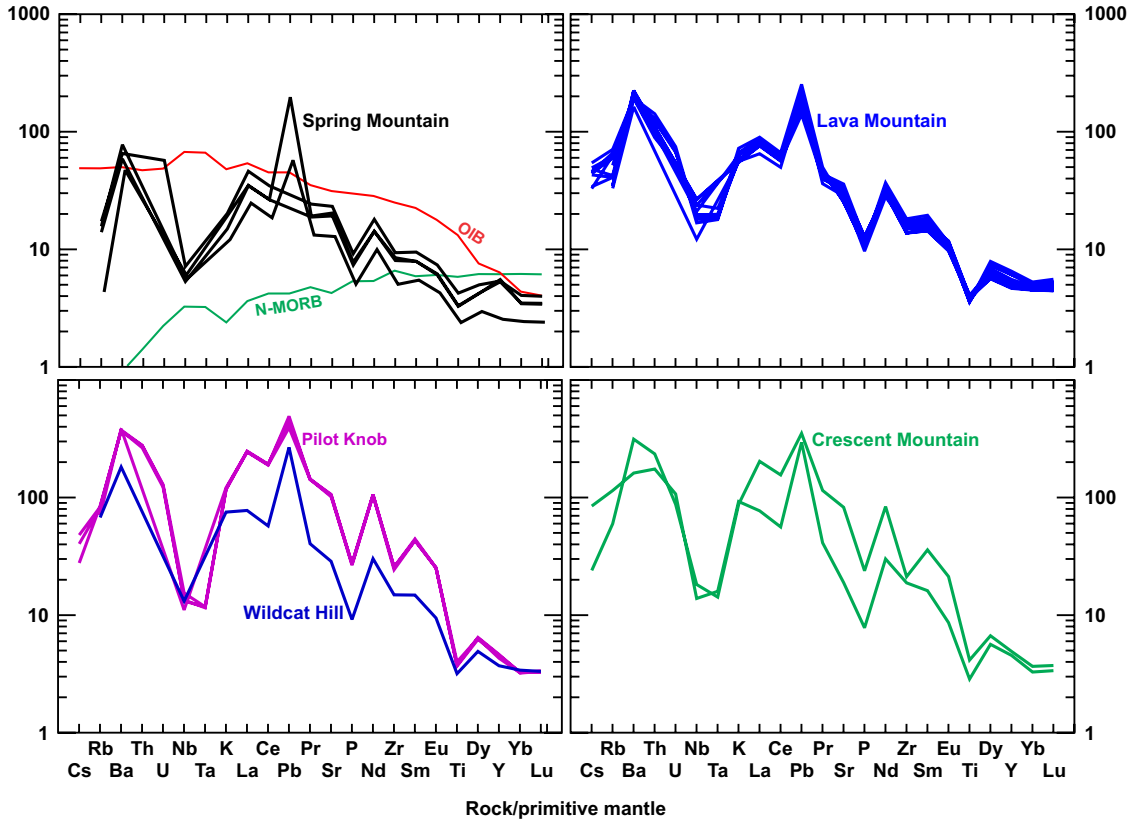

Figure 10. Primitive mantle–normalized trace element variations of Upper Wind River Basin volcanic field rocks with a full suite of rare earth element data, after Sun and McDonough (1989). OIB—ocean-island basalt; N-MORB—normal mid-ocean-ridge basalt (Sun and McDonough, 1989).

flat to curved HREE patterns in relatively primitive rocks (e.g., basalt, lamprophyre) is typically attributed to partial melting in the presence of garnet. The degree of LREE enrichment is also consistent with melting of LREE-enriched lithospheric mantle.

DISCUSSION

Preliminary Petrogenetic Constraints of UWRB Magmas

Our petrographic evidence indicates that UWRB rocks were affected by small degrees of crustal contamination. The Lava Mountain samples have major element trends displaying primarily positive or negative linear trends with SiO_2 (Fig. 8) and have enriched incompatible trace element characteristics relative to UWRB basalts (Fig. 10) consistent with an origin affected by fractional crystallization processes. Nonetheless, anhedral, partially resorbed xenocrystic microcline is observed in a Lava Mountain andesite (sample AD14-7) and suggests interaction with crust, as do quartz and plagioclase (with reaction rims) xenocrysts in other andesites, basaltic andesites, and dacites. One potential assimilant is the Archean Wyoming craton crust, which consists of a combination of gneiss, granodiorite, and metasedimentary rocks (Keefer, 1957; Foster et al., 2006). Geochemical evidence also suggests some amount of crustal contamination. For example, average Ce/Pb is 26.1 in N-MORB and 25 in OIB, while values <4 characterize the continental crust (Niu and O'Hara, 2003; Rudnick and Gao, 2003). In the Spring Mountain basalts, Ce/Pb is ~3–8 and in the other rocks reaches slightly higher values (~5–12). Similar relationships are present with Nb/U, another trace element ratio that in basalts (Nb/U > 40; Niu and O'Hara, 2003) can indicate crustal interaction (crustal Nb/U < 4; Rudnick and Gao, 2003). However, it is possible that these ratios in the UWRB rocks also reflect enrichments and depletions of these elements due to earlier subduction-related metasomatism of the underlying mantle. For example,

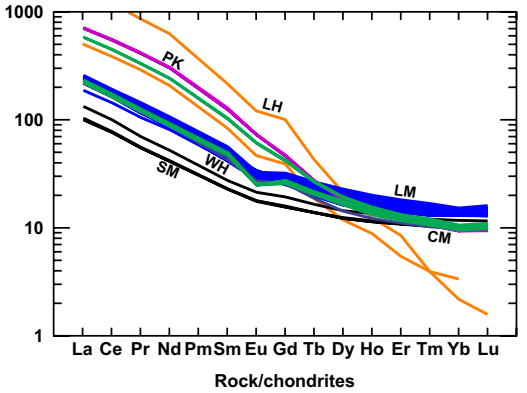

Figure 11. Upper Wind River Basin volcanic field rare earth element compositions normalized to chondrite after Sun and McDonough (1989). PK—Pilot Knob (purple lines); WH—Wildcat Hill (dark blue); LM—Lava Mountain (lighter blue); SM—Spring Mountain (black); CM—Crescent Mountain (green). LH—representative Leucite Hills alkaline magmas for comparison (orange lines; Mirnejad and Bell, 2006).

Cenozoic basalts and andesites erupted adjacent to the Colorado Plateau in the southwestern USA have Ce/Pb ranging from 4.6 to 37 (Kempton et al., 1991). Kempton et al. (1991) demonstrated that the geochemical and Sr-Nd-Pb isotopic characteristics of these rocks reflect a derivation via melting of Archean lithosphere affected by a prior history of subduction-related fluid and melt enrichment and not contamination of asthenospheric melts with local and/or regional crust. Thus, while minor crustal assimilation affected some of the UWRB rocks, it may not have significantly changed the bulk chemistry of the least evolved rocks (e.g., Spring Mountain basalts, Pilot Knob).

Downey (2015) developed a preliminary two-step model to explain the generation of the evolved Lava Mountain magmas: (1) closed-system fractional crystallization of basalt to basaltic andesite and dacite, followed by (2) magma mixing of basaltic andesite and dacite (plus minor assimilation) to generate the andesite. The textures observed in the andesites and their essentially aphyric nature (e.g., ~85%–90% groundmass) are consistent with magma mixing coupled with relatively quick ascent and eruption (Johnson and Grunder, 2000; Brueseke and Hart, 2009). This model is also consistent with stratigraphic evidence that the initial and basal eruptions at Lava Mountain alternated between basaltic andesitic and dacite, followed by andesite eruptions that form the greatest volume of the volcano and the final pyroclastic phase (Downey, 2015). Additional petrologic details for the UWRB rocks are beyond the focus of this contribution.

A continental magmatic arc was present in northwest Wyoming in the Eocene, and it has been suggested that subduction-related magmatism also affected the region during the Proterozoic (Dudás et al., 1987; Mueller and Wooden, 1988; Carlson and Irving, 1994; Feeley, 2003). Modern subduction processes produce magmas that are enriched in LREEs and LILEs and depleted in HREEs and HFSEs (Smithies et al., 2004); all UWRB samples have these characteristic enrichments and depletions. Figure 12 illustrates these characteristics and compares the UWRB rocks to Yellowstone Plateau volcanic field basalts (Fig. 12A) and representative samples of the Jackson Hole volcanics and Leucite Hills (Fig. 12B). Clearly the UWRB rocks, including the Spring Mountain basalts high in Mg, Ni, and Cr, are geochemically distinct compared to basalts from the Yellowstone Plateau volcanic field (Fig. 12A), which generally lack the LILE enrichments and HFSE depletions that characterize the UWRB rocks. Similar trace element patterns are present in the ca. 8.5–8 Ma Jackson

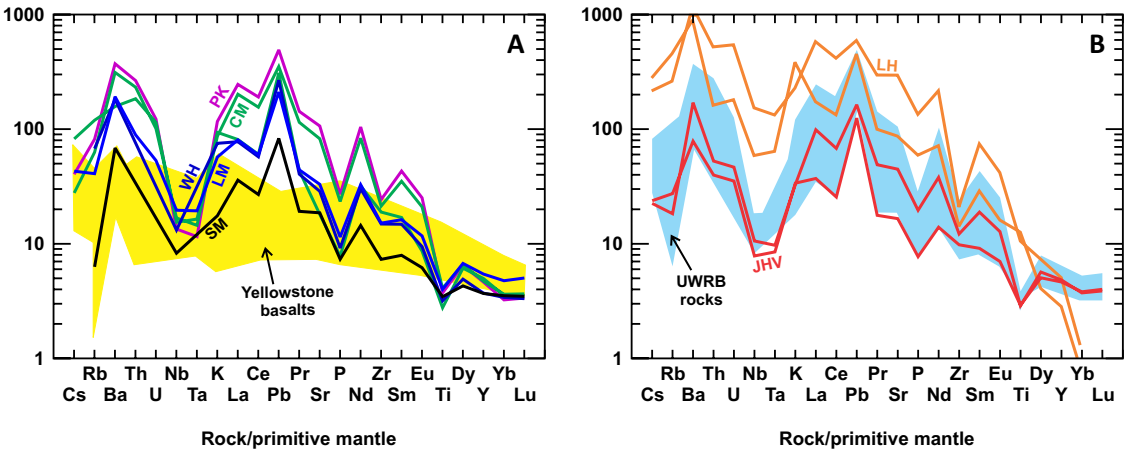

Figure 12. Primitive mantle–normalized trace element variations of representative Upper Wind River Basin volcanic field (UWRB) rocks as in Figure 10, compared to Yellowstone basalts (yellow shaded field; Hildreth, et al., 1991; Christiansen, 2001) (PK—Pilot Knob; WH—Wildcat Hill; LM—Lava Mountain; SM—Spring Mountain; CM—Crescent Mountain) (A) and representative samples of Jackson Hole volcanics (JHV, red lines; Adams, 1997) and Leucite Hills alkaline magmas (LH, orange lines; Mirnejad and Bell, 2006) (B); UWRB rocks define the blue shaded field in B.

Hole volcanics (Adams, 1997) (Fig. 12B), which would be expected if they have a similar origin as UWRB rocks. Furthermore, Leucite Hills volcanic rocks also exhibit similar patterns (Fig. 12B), which Mirnejad and Bell (2006) interpreted, based on other lines of evidence, as reflecting their derivation from metasomatized Wyoming craton lithospheric mantle. Adams (2014) also suggested that the Jackson Hole volcanics were derived from a lithospheric mantle source, based on their bulk chemistry and $^{87}Sr/^{86}Sr$ (0.7061–0.7104) and ε_{Nd} (–18.5 to –22.5) values. The subduction signature in UWRB rocks (and these similar regional volcanics) must result from the prior history of subduction in this part of North America because of the age of the UWRB rocks and their location in Wyoming, i.e., thousands of kilometers inboard from active Miocene to modern subduction. Thus, it is possible that the UWRB rocks represent either direct melting of Wyoming craton lithospheric mantle (e.g., Spring Mountain basalts and Pilot Knob) or evolution from a mafic melt originally derived from lithospheric mantle (e.g., Lava Mountain and Crescent Mountain). More detailed study involving radiogenic isotopes is needed to test these hypotheses and resolve the characteristics and relative roles of mantle and crustal reservoirs in UWRB magmatism.

The Yellowstone Hotspot: Trigger for UWRB Volcanism?

As discussed earlier, northwestern Wyoming, eastern Idaho, and southwestern Montana were affected by two phases of extension during the last ~18 m.y.: (1) mid-Miocene extension that is likely due to collapse of Laramide and Sevier uplifts (Constenius, 1996), and (2) a later <ca. 5 Ma phase that could result from the North American plate moving over the Yellowstone hotspot tail (Anders et al., 2009). The primary effect of the Yellowstone hotspot tail on the North American lithosphere is significant uplift in a generally parabolic shape that is typical for plumes (Anders et al., 1989; Anders and Sleep, 1992; Pierce and Morgan, 1992; Wegmann et al., 2007; Smith et al., 2009; Obrebski et al., 2011), coupled with increased heat flow and melt production. Evidence for ~1 km of uplift in the upper Wind River Basin is best exhibited by the narrow, deep canyons that have been cut into the highly erodible Eocene package, and the regional erosion surface that formed on the thick package of Eocene Absaroka strata on which the UWRB volcanics erupted (Fig. 4) (Pierce and Morgan, 1992; 2009). Furthermore, the exposure of the Pilot Knob and Wildcat Hill intrusions also demonstrate uplift and exhumation during the last few million years. Anders et al. (1989), Pierce and Morgan (1992), and Anders et al. (2009) suggested that there was a wave of extensional activity before voluminous caldera-forming silicic volcanism began at any given location along the Snake River Plain, attributed to the migration of the North American plate over the Yellowstone plume tail. Rodgers et al. (1990, 2002) documented this extension north and south of the eastern Snake River Plain and attributed it to the aforementioned migration. Vogl et al. (2014) also connected ca. 11–8 Ma uplift followed by normal faulting north of the Snake River Plain in Idaho to volcanism and hotspot passage related to the ca. 10.4–6.6 Ma Picabo volcanic field (Drew et al., 2013). Similar links are also documented in southwestern Montana (Fritz and Sears, 1993; Sears et al., 2009). In contrast, Brueseke et al. (2014) linked eastward-migrating ca. 16–12 Ma Jarbidge Rhyolite volcanism in northeastern Nevada to coeval migrating Basin and Range extension that predated major hotspot-related volcanism at a given longitude.

Pierce and Morgan (2009, p. 13) defined the active region of extension around Yellowstone as a zone of "incipient activity (or rejuvenation)" that refers to neotectonic activity along active or previously active faults and seismicity that surrounds and extends from Yellowstone (e.g., the tectonic parabola or Yellowstone crescent of high terrain; Fig. 1). The leading front of the present-day active belt of extension is east of the Absaroka Range and bisects the Wind River Basin and Wind River Range (Fig. 1), encompassing the upper Wind River Basin. Figure 1 also depicts inferred topographic swells associated with the Heise and Picabo volcanic fields (Smith et al., 2009), assuming a similar ~100–200-km-wide footprint between the leading front and back of the current tectonic parabola (Yellowstone crescent of high terrain) east and northeast of the respective volcanic field (Anders et al., 1989). Regardless of whether the tectonic parabola is caused by Yellowstone hotspot–North American plate interaction or instead due to Basin and Range extension, ample evidence demonstrates that it exists and has migrated northeast across the North American plate. Geophysical studies document high heat flow and increased mantle and crustal temperatures associated with the hotspot, now adjacent to and affecting the upper Wind River Basin (Kelbert et al., 2012; Huang et al., 2015). Thus, the combination of hotter mantle and crust, coupled with extension and uplift, provided ample opportunities for UWRB melt production and volcanism during the last ~5 m.y.

We suggest that UWRB magmatism was primarily triggered by temperature increase and lithospheric extension associated with the Yellowstone hotspot tail and its tectonic parabola as it moved (relative to North American plate motion) from Idaho to its current location in northwest Wyoming. This aligns with the model of Adams (2014) based on seismic attenuation tomography, where melt generation would have occurred due to thermal input from the Yellowstone plume, coupled with adiabatic decompression of hydrous lithospheric mantle. The general spatio-temporal relationship between the Jackson Hole volcanics and UWRB rocks depicted in Figure 1 is consistent with this hypothesis, where volcanism generally gets younger to the east. If this relationship were solely related to the movement of the plate over the hotspot tail and the resulting tectonic parabola, we would expect a simple eastward age progression. However, the age relations of dated UWRB rocks do not conform to a simple progression, even though all are younger than the Jackson Hole volcanics. For example, Pilot Knob, Crescent Mountain, and Lava Mountain are all found just west of Spring Mountain, and Lava Mountain itself is much younger than Pilot Knob even though both exist in essentially the same location. Undoubtedly some other control on magma emplacement is also playing a role on where UWRB magmatism occurred. We propose that this is due to crustal heterogeneities imparted in the region during prior Laramide and Sevier compression. Reactivation of Mesozoic faults because of Basin and Range extension and extension due to the Yellowstone hotspot tectonic parabola

would provide ample locations to focus magma during UWRB magmatism. Love (1939), Keefer (1955), and Winterfeld and Conrad (1983) described southeast-trending normal faults, such as the Bear Creek fault, just east and north of Spring Mountain which lie parallel to the strike of major Mesozoic thrust faults that front the Washakie uplift (Fig. 2). Moreover, Love et al. (1979) mapped southeast-trending normal faults that extend to the southeast of the UWRB in the Wind River Range (Figs. 1, 2). These are all likely the result of post-Laramide extensional collapse of the Wind River uplift, given their southeast trend that is parallel to major compressional structures in Paleozoic to Mesozoic rocks in the Wind River and Washakie uplifts (Ketner et al., 1966; Winterfeld and Conrad, 1983). Lava Mountain (as well as Pilot Knob and Wildcat Hill) lies between the faults in the Wind River Range and along the strike of the Upper Yellowstone fault zone, one of the southeast-trending normal fault–bounded corridors that extends south from Yellowstone Lake (Figs. 1, 2; Pierce and Morgan, 1992; Christiansen, 2001). Earthquake epicenter locations from 1950 to 28 February 2017 downloaded from the U.S. Geological Survey earthquake database (https://earthquake.usgs.gov/earthquakes/map/) also show that recent earthquakes have occurred just northwest and southeast of Lava Mountain near mapped normal faults (Love and Love, 1983; Machette et al., 2001), further defining this corridor as a zone of active faulting. Moreover, Protska et al. (1979) and Rohrer (1966) documented Pliocene(?) mafic dikes that trend 10° and cut Eocene strata near Crescent Mountain. Protska et al. (1979) hypothesized that these dikes, Crescent Mountain, and Lava Mountain all were emplaced or erupted along a lithosphere-scale fracture system. This feature and the corridor of active faulting that extends northwest and southeast of Lava Mountain intersect at Lava Mountain–Pilot Knob, indicating that this junction has been a locus of magmatism during the last 3.6 m.y. Finally, normal faulting at Spring Mountain provides the clearest evidence of this connection between UWRB magmatism and extension. The vent locations at Spring Mountain are fault controlled, and the basalt erupted via these fissures. The styles of magmatism we document in the UWRB are consistent with prior observations that monogenetic volcanism is primarily associated with extension and increased rates of regional differential stresses (Takada, 1994; Cashman and Sparks, 2013).

In summary, field relations and modern seismicity provide unambiguous evidence that UWRB magmatism is spatially related to local and regional normal faults, some of which must reflect preexisting crustal heterogeneity that was imparted before active upwelling and faulting associated with Basin and Range extension and the Yellowstone hotspot affected the upper Wind River Basin. This relationship also explains the location and timing of the Jackson Hole volcanics just west of the UWRB, and the ca. 7–6 Ma dacitic Carlton Creek Volcanics and Palisades Dam–Calamity Point Andesite in eastern Idaho (Armstrong et al., 1980; Anders et al., 2009, 2014; Price, 2009; Fig. 1). The Carlton Creek Volcanics $^{40}Ar/^{39}Ar$ age determinations (Price, 2009) were calculated using the Fish Canyon Tuff flux monitor with an age of 27.84 Ma, and the Palisades Dam–Calamity Point Andesite age was determined by the K-Ar method (Armstrong et al., 1980), hence approximate ages and ranges are presented and used for comparison.

The Jackson Hole volcanic sequence crops out at the southern end of Jackson Hole, near where major Laramide and Sevier faults (e.g., Cache Creek and Jackson thrusts, respectively) intersect younger Basin and Range structures like the Teton normal fault, in a zone of differential extension (Adams, 1997). The Carlton Creek Volcanics are along the northern edge of the Big Hole Mountain Mountains, and the Palisades Dam–Calamity Point Andesite is along the eastern Caribou Range, adjacent to Basin and Range normal faults (Anders et al., 2009; Price, 2009). These faults are parallel to major north-northwest–trending thrust faults that were active during the Sevier orogeny (Yonkee and Weil, 2015), suggesting that preexisting structures (e.g., Laramide-Sevier thrust faults) controlled the location of Cenozoic normal faulting and magmatism, similar to what we propose for the upper Wind River Basin. Price (2009) confirmed that Carlton Creek volcanism occurred at the same time or just before major caldera-forming silicic volcanism initiated on the Snake River Plain in the Heise volcanic field. This is the same general age relationship we document in the upper Wind River Basin, where most UWRB magmatism occurs prior to major volcanism at Yellowstone, and is essentially the same relationship noted between widespread Miocene rhyolite volcanism across northeastern Nevada and central Snake River Plain caldera-forming volcanism to the north in Idaho (Brueseke et al., 2014). While ample evidence exists that Miocene extension occurred in the greater Yellowstone region and along the trend of the Snake River Plain in Idaho, a younger episode of eastward-migrating extension also affected the greater Yellowstone region and is associated with a similar eastward migration of magmatism, prior to Yellowstone volcanism. Lava Mountain is the youngest manifestation of these processes. As a result, it appears that in multiple locations across most of the length of the Yellowstone hotspot track through North America, major caldera-forming silicic activity was preceded, at a given longitude, by typically smaller-volume volcanism, likely associated with uplift and extension. We suggest that similar relations should characterize other examples of continental hotspots as exhibited in the age-progression pattern for the proposed Anahim hotspot track in British Columbia (Canada) (Kuehn et al., 2015), and can be used to identify them in other locations in both the modern and past geological records.

CONCLUSIONS

1. New $^{40}Ar/^{39}Ar$ ages coupled with existing K-Ar results indicate that <ca. 5 Ma igneous activity occurred in the upper Wind River Basin, Wyoming, and define the Upper Wind River Basin volcanic field (UWRB). This includes 4.8 Ma volcanism at Spring Mountain and ca. 3.5 Ma magmatism at Pilot Knob and Crescent Mountain, both of which predate the formation of the Yellowstone Plateau volcanic field. Lava Mountain, the youngest UWRB volcano that we have studied, formed at 397 ± 48 ka, which postdates third-cycle caldera-forming activity in the Yellowstone Plateau volcanic field.

2. Prior geological mapping suggested that Lava Mountain is a basaltic volcano, however new major element chemistry demonstrates that the volcano is not basaltic, but instead formed via eruptions of calc-alkaline basaltic andesite,

andesite, and dacite. Other intermediate-composition magmatism occurred at Pilot Knob (alkaline lamprophyre), Wildcat Hill (calc-alkaline andesite to dacite), and Crescent Mountain (calc-alkaline basaltic andesite and dacite), while eruptions of tholeiitic basalt characterize Spring Mountain. UWRB igneous rocks have trace element characteristics typically associated with subduction (e.g., LILE enrichment, HFSE depletions), though they erupted in a location thousands of kilometers inland from the closest active volcanic arc. They are also geochemically dissimilar from young basaltic volcanism at Yellowstone. Other <9 Ma regionally exposed igneous rocks (e.g., Jackson Hole volcanics) have identical geochemical characteristics, as do magmas from the Leucite Hills, Wyoming, all of which have previously been attributed to melting of Archean lithospheric mantle.

3. UWRB magmas were emplaced and erupted along normal fault zones associated with regional extension, some of which likely reflect preexisting structural heterogeneity that originally formed via Mesozoic compressional faulting. We suggest that this process is related to interaction between the North American plate and the progression of the tectonic parabola associated with the Yellowstone hotspot, generally ahead of, and out of sequence with, voluminous silicic magmatism associated with the hotspot on the Snake River Plain and at the Yellowstone Plateau volcanic field. This style of out-of-sequence, hotspot-related volcanism can be used to identify hotspots in other locations.

ACKNOWLEDGMENTS

This work was motivated by many discussions about upper Wind River Basin geology among M. Brueseke, W. Hart, C. Haley, and B. Currie at Miami University's geology field camp (Dubois, Wyoming). Brueseke, Downey, and Dodd thank the Wells family for allowing us to stay at the Timberline Ranch (Dubois) during fieldwork, and John Morton at Miami University for assistance with analytical geochemistry. We thank Associate Guest Editor Ben Ellis, Dave Hacker, an anonymous reviewer, and Editor Shan de Silva for helpful comments and/or handling of this manuscript. This research was funded by: a Tobacco Root Geological Society Field Scholarship (Downey), a Wyoming Geological Association J.D. Love scholarship (Downey), a Kansas Geological Foundation research scholarship (Downey), a Society of Economic Geologists student research grant (Dodd), a Kansas State University Small Research Grant (Brueseke), and the Janet and Elliot Baines Professorship at Miami University (Hart).

REFERENCES CITED

Adams, D.C., 1997, Miocene calc-alkaline volcanism in southern Jackson Hole, Wyoming: Evidence of subduction-related volcanism [M.S. thesis]: Bozeman, Montana State University, 127 p.

Adams, D.C., 2014, Intermediate volcanism associated with the Yellowstone hotspot, southeastern Idaho and western Wyoming: Geological Society of America Abstracts with Programs, v. 46, no. 5, p. 94.

Anders, M.H., and Sleep, N.H., 1992, Magmatism and extension: The thermal and mechanical effects of the Yellowstone hotspot: Journal of Geophysical Research, v. 97, p. 15,379–15,393, https://doi.org/10.1029/92JB01376.

Anders, M.H., Geissman, J.W., Piety, L.A., and Sullivan, J.T., 1989, Parabolic distribution of circum-eastern Snake River Plain seismicity and latest Quaternary faulting: Migratory pattern and association with the Yellowstone hotspot: Journal of Geophysical Research, v. 94, p. 1589–1621, https://doi.org/10.1029/JB094iB02p01589.

Anders, M.H., Saltzman, J., and Hemming, S.R., 2009, Neogene tephra correlations in eastern Idaho and Wyoming: Implications for Yellowstone hotspot-related volcanism and tectonic activity: Geological Society of America Bulletin, v. 121, p. 837–856, https://doi.org/10.1130/B26300.1.

Anders, M.H., Rodgers, D.W., Hemming, S.R., Saltzman, J., Divenere, V.J., Hagstrum, J.T., Embree, G.F., and Walter, R.C., 2014, A fixed sublithospheric source for the late Neogene track of the Yellowstone hotspot: Implications of the Heise and Picabo volcanic fields: Journal of Geophysical Research: Solid Earth, v. 119, p. 2871–2906, https://doi.org/10.1002/2013JB010483.

Armstrong, R.L., Harakal, J.E., and Neill, W.M., 1980, K-Ar dating of Snake River Plain (Idaho) volcanic rocks—New results: Isochron-West, v. 27, p. 5–10.

Barnosky, A.D., and Labar, W.J., 1989, Mid-Miocene (Barstovian) environmental and tectonic setting near Yellowstone Park, Wyoming and Montana: Geological Society of America Bulletin, v. 101, p. 1448–1456, https://doi.org/10.1130/0016-7606(1989)101<1448:MMBEAT>2.3.CO;2.

Benowitz, J.A., Layer, P.W., and Vanlaningham, S., 2014, Persistent long-term (c. 24 Ma) exhumation in the Eastern Alaska Range constrained by stacked thermochronology, *in* Jourdan, F., Mark, D.F., and Verati, C., eds., Advances in $^{40}Ar/^{39}Ar$ Dating: From Archaeology to Planetary Sciences: Geological Society of London Special Publication 378, p. 225–243, https://doi.org/10.1144/SP378.12.

Bercovici, D., and Mahoney, J., 1994, Double flood basalts and plume head separation at the 660-kilometer discontinuity: Science, v. 266, p. 1367–1369, https://doi.org/10.1126/science.266.5189.1367.

Blackstone, D.L., 1966, Pliocene vulcanism, southern Absaroka Mountains, Wyoming: University of Wyoming Contributions to Geology, v. 5, no. 1, p. 21–30.

Brueseke, M.E., and Hart, W.K., 2009, Intermediate composition magma production in an intracontinental setting: Unusual andesites and dacites of the mid-Miocene Santa Rosa–Calico volcanic field, northern Nevada: Journal of Volcanology and Geothermal Research, v. 188, p. 197–213, https://doi.org/10.1016/j.jvolgeores.2008.12.015.

Brueseke, M.E., Callicoat, J.S., Hames, W., and Larson, P.B., 2014, Mid-Miocene rhyolite volcanism in northeastern Nevada: The Jarbidge Rhyolite and its relationship to the Cenozoic evolution of the northern Great Basin (USA): Geological Society of America Bulletin, v. 126, p. 1047–1067, https://doi.org/10.1130/B30736.1.

Burbank, D.W., and Barnosky, A.D., 1990, The magnetochronology of Barstovian mammals in southwestern Montana and implications for the initiation of Neogene crustal extension in the northern Rocky Mountains: Geological Society of America Bulletin, v. 102, p. 1093–1104, https://doi.org/10.1130/0016-7606(1990)102<1093:TMOBMI>2.3.CO;2.

Camp, V.E., and Ross, M.E., 2004, Mantle dynamics and genesis of mafic magmatism in the intermontane Pacific Northwest: Journal of Geophysical Research, v. 109, B08204, https://doi.org/10.1029/2003JB002838.

Camp, V.E., Pierce, K.L., and Morgan, L.A., 2015, Yellowstone plume trigger for Basin and Range extension, and dike injection oblique to regional stress along the Nevada-Columbia Basin magmatic belt: Geosphere, v. 11, p. 203–225, https://doi.org/10.1130/GES01051.1.

Carlson, R.W., and Hart, W.K., 1987, Crustal genesis on the Oregon Plateau: Journal of Geophysical Research, v. 92, p. 6191–6206, https://doi.org/10.1029/JB092iB07p06191.

Carlson, R.W., and Irving, A.J., 1994, Depletion and enrichment history of subcontinental lithospheric mantle: An Os, Sr, Nd and Pb isotopic study of xenoliths from the northwestern Wyoming craton: Earth and Planetary Science Letters, v. 126, p. 457–472, https://doi.org/10.1016/0012-821X(94)90124-4.

Carmichael, I.S.E., 1967, The mineralogy and petrology of the volcanic rocks from the Leucite Hills, Wyoming: Contributions to Mineralogy and Petrology, v. 15, p. 24–66, https://doi.org/10.1007/BF01167214.

Cashman, K.V., and Sparks, R.S.J., 2013, How volcanoes work: A 25 year perspective: Geological Society of America Bulletin, v. 125, p. 664–690, https://doi.org/10.1130/B30720.1.

Christiansen, R.L., 1984, Yellowstone magmatic evolution: Its bearing on understanding large-volume explosive volcanism, *in* Explosive Volcanism: Inception, Evolution, and Hazards: Washington, D.C., The National Academy Press, p. 84–95.

Christiansen, R.L., 2001, The Quaternary and Pliocene Yellowstone Plateau volcanic field of Wyoming, Idaho, and Montana: U.S. Geological Survey Professional Paper 729-G, 120 p.

Christiansen, R.L., Foulger, G.R., and Evans, J.R., 2002, Upper-mantle origin of the Yellowstone hotspot: Geological Society of America Bulletin, v. 114, p. 1245–1256, https://doi.org/10.1130/0016-7606(2002)114<1245:UMOOTY>2.0.CO;2.

Christiansen, R.L., Lowenstern, J.B., Smith, R.B., Heasler, H., Morgan, L.A., Nathenson, M., Mastin, L.G., Muffler, L.J.P., and Robinson, J.E., 2007, Preliminary assessment of volcanic and hydrothermal hazards in Yellowstone National Park and vicinity: U.S. Geological Survey Open File Report 2007-1071, 94 p.

Colgan, J.P., and Henry, C.D., 2009, Rapid middle Miocene collapse of the Mesozoic orogenic plateau in north-central Nevada: International Geology Review, v. 51, p. 920–961, https://doi.org/10.1080/00206810903056731.

Constenius, K.N., 1996, Late Paleogene extensional collapse of the Cordilleran foreland fold and thrust belt: Geological Society of America Bulletin, v. 108, p. 20–39, https://doi.org/10.1130/0016-7606(1996)108<0020:LPECOT>2.3.CO;2.

Courtillot, V., Davaille, A., Besse, J., and Stock, J., 2003, Three distinct types of hotspots in the Earth's mantle: Earth and Planetary Science Letters, v. 205, p. 295–308, https://doi.org/10.1016/S0012-821X(02)01048-8.

de Silva, S., and Lindsay, J.M., 2015, Primary volcanic landforms, *in* Sigurdsson, H., Houghton, B., McNutt, S.R., Rymer, H., and Stix, J., eds., The Encyclopedia of Volcanoes (second edition): Amsterdam, Elsevier, p. 273–297, https://doi.org/10.1016/B978-0-12-385938-9.00015-8.

Dodd, Z.C., 2015, Petrogenesis and rare earth element economic potential of Pilot Knob, a Pliocene(?) alkaline intrusive complex in the Togwotee Pass region, northwestern Wyoming (USA) [M.S. thesis]: Manhattan, Kansas State University, 75 p.

Downey, A.C., 2015, Cenozoic mafic to intermediate volcanism at Lava Mountain and Spring Mountain, Upper Wind River Basin, Wyoming [M.S. thesis]: Manhattan, Kansas State University, 99 p.

Drew, D.L., Bindeman, I.N., Watts, K.E., Schmitt, A.K., Fu, B., and McCurry, M., 2013, Crustal-scale recycling in caldera complexes and rift zones along the Yellowstone hotspot track: O and Hf isotopic evidence in diverse zircons from voluminous rhyolites of the Picabo volcanic field, Idaho: Earth and Planetary Science Letters, v. 381, p. 63–77, https://doi.org/10.1016/j.epsl.2013.08.007.

Dudás, F.O., Carlson, R.W., and Eggler, D.H., 1987, Regional Middle Proterozoic enrichment of the subcontinental mantle source of igneous rocks from central Montana: Geology, v. 15, p. 22–25, https://doi.org/10.1130/0091-7613(1987)15<22:RMPEOT>2.0.CO;2.

Duffield, W.A., and Dalrymple, G.B., 1990, The Taylor Creek Rhyolite of New Mexico: A rapidly emplaced field of lava domes and flows: Bulletin of Volcanology, v. 52, p. 475–487, https://doi.org/10.1007/BF00268927.

Ellis, B.S., Szymanowski, D., Wotzlaw, J.F., Schmitt, A.K., Bindeman, I.N., Troch, J., Harris, C., and Guillong, M., 2017, Post-caldera volcanism at the Heise volcanic field: Implications for petrogenetic models: Journal of Petrology, v. 58, p. 115–136, https://doi.org/10.1093/petrology/egx007.

Fan, M., DeCelles, P.G., Gehrels, G.E., Dettman, D.L., Quade, J., and Peyton, S.L., 2011, Sedimentology, detrital zircon geochronology, and stable isotope geochemistry of the lower Eocene strata in the Wind River Basin, central Wyoming: Geological Society of America Bulletin, v. 123, p. 979–996, https://doi.org/10.1130/B30235.1.

Feeley, T.C., 2003, Origin and tectonic implications of across-strike geochemical variations in the Eocene Absaroka volcanic province, United States: The Journal of Geology, v. 111, p. 329–346, https://doi.org/10.1086/373972.

Foster, D.A., Mueller, P.A., Mogk, D.W., Wooden, J.L., and Vogl, J.J., 2006, Proterozoic evolution of the western margin of the Wyoming craton: Implications for the tectonic and magmatic evolution of the northern Rocky Mountains: Canadian Journal of Earth Sciences, v. 43, p. 1601–1619, https://doi.org/10.1139/e06-052.

Fouch, M.J., 2012, The Yellowstone hotspot: Plume or not?: Geology, v. 40, p. 479–480, https://doi.org/10.1130/focus052012.1.

Fritz, W.J., and Sears, J.W., 1993, Tectonics of the Yellowstone hotspot wake in southwestern Montana: Geology, v. 21, p. 427–430, https://doi.org/10.1130/0091-7613(1993)021<0427:TOTYHW>2.3.CO;2.

Gaschnig, R.M., Vervoort, J.D., Lewis, R.S., and Tikoff, B., 2011, Isotopic evolution of the Idaho batholith and Challis intrusive province, northern US Cordillera: Journal of Petrology, v. 52, p. 2397–2429, https://doi.org/10.1093/petrology/egr050.

Hieronymus, C.F., and Bercovici, D., 2001, A theoretical model of hotspot volcanism: Control on volcanic spacing and patterns via magma dynamics and lithospheric stresses: Journal of Geophysical Research, v. 106, p. 683–702, https://doi.org/10.1029/2000JB900355.

Hildreth, W., Halliday, A.N., and Christiansen, R.L., 1991, Isotopic and chemical evidence concerning the genesis and contamination of basaltic and rhyolitic magma beneath the Yellowstone Plateau volcanic field: Journal of Petrology, v. 32, p. 63–138, https://doi.org/10.1093/petrology/32.1.63.

Huang, H.-H., Lin, F.-C., Schmandt, B., Farrell, J., Smith, R.B., and Tsai, V.C., 2015, The Yellowstone magmatic system from the mantle plume to the upper crust: Science, v. 348, p. 773–776, https://doi.org/10.1126/science.aaa5648.

Jean, M.M., Hanan, B.B., and Shervais, J.W., 2014, Yellowstone hotspot–continental lithosphere interaction: Earth and Planetary Science Letters, v. 389, p. 119–131, https://doi.org/10.1016/j.epsl.2013.12.012.

Johnson, D.M., Hooper, P.R., and Conrey, R.M., 1999, XRF analysis of rocks and minerals for major and trace elements on a single low dilution Li-tetraborate fused bead: Advances in X-ray Analysis, v. 41, p. 843–867.

Johnson, J.A., and Grunder, A.L., 2000, The making of intermediate composition magma in a bimodal suite: Duck Butte Eruptive Center, Oregon, USA: Journal of Volcanology and Geothermal Research, v. 95, p. 175–195, https://doi.org/10.1016/S0377-0273(99)00125-0.

Katoh, S., Beyene, Y., Tetsumaru, I., Hyodo, H., Hyodo, M., Yagi, K., Gouzu, C., WoldeGabriel, G., Hart, W.K., Ambrose, S.H., Nakaya, H., Bernor, R.L., Boisserie, J.-R., Bibi, F., Saegusa, H., Sasaki, T., Sano, K., Asfaw, B., and Suwa, G., 2016, New geological and palaeontological age constraint for the gorilla–human lineage split: Nature, v. 530, p. 215–218, https://doi.org/10.1038/nature16510.

Keefer, W.R., 1955, Geologic map of the Du Noir area, Fremont County, Wyoming: U.S. Geological Survey Oil and Gas Investigation Map 166, scale 1:48,000.

Keefer, W.R., 1957, Geology of the Du Noir area, Fremont County, Wyoming: U.S. Geological Survey Professional Paper 294-E, 72 p.

Keefer, W.R., 1970, Structural geology of the Wind River Basin, Wyoming: U.S. Geological Survey Professional Paper 495-D, 40 p.

Kelbert, A., Egbert, G.D., and deGroot-Hedlin, C., 2012, Crust and upper mantle electrical conductivity beneath the Yellowstone Hotspot Track: Geology, v. 40, p. 447–450, https://doi.org/10.1130/G32655.1.

Kempton, P.D., Fitton, J.D., Hawkesworth, C.J., and Ormerod, D.S., 1991, Isotopic and trace element constraints on the composition and evolution of the lithosphere beneath the southwestern United States: Journal of Geophysical Research, v. 96, p. 13,713–13,735, https://doi.org/10.1029/91JB00373.

Ketner, K.B., Keefer, W.R., Fisher, F.S., and Smith, D.L., 1966, Mineral resources of the Stratified Primitive Area, Wyoming: U.S. Geological Survey Bulletin 1230-E, 56 p.

Konstantinou, A., Valley, J., Strickland, A., Miller, E.L., Fisher, C., Vervoort, J., and Wooden, J., 2013, Geochemistry and geochronology of the Jim Sage volcanic suite, southern Idaho: Implications for Snake River Plain magmatism and its role in the history of Basin and Range extension: Geosphere, v. 9, p. 1681–1703, https://doi.org/10.1130/GES00948.1.

Kuehn, C., Guest, B., Russell, J.K., and Benowitz, J.A., 2015, The Satah Mountain and Baldface Mountain volcanic fields: Pleistocene hot spot volcanism in the Anaheim Volcanic Belt, west-central British Columbia, Canada: Bulletin of Volcanology, v. 77, 19, https://doi.org/10.1007/s00445-015-0907-1.

Lageson, D.R., Adams, D.C., Morgan, L., Pierce, K.L., and Smith, R.B., 1999, Neogene-Quaternary tectonics and volcanism of southern Jackson Hole, Wyoming and southeastern Idaho, *in* Hughes, S.S., and Thackray, G.D., eds., Guidebook to the Geology of Eastern Idaho: Pocatello, Idaho Museum of Natural History, p. 115–130.

Lange, R.A., Carmichael, I.S.E., and Hall, C.M., 2000, $^{40}Ar/^{39}Ar$ chronology of the Leucite Hills, Wyoming: Eruption rates, erosion rates, and an evolving temperature structure of the underlying mantle: Earth and Planetary Science Letters, v. 174, p. 329–340, https://doi.org/10.1016/S0012-821X(99)00267-8.

Layer, P.W., Hall, C.M., and York, D., 1987, The derivation of $^{40}Ar/^{39}Ar$ age spectra of single grains of hornblende and biotite by laser step heating: Geophysical Research Letters, v. 14, p. 757–760, https://doi.org/10.1029/GL014i007p00757.

Le Bas, M.J., and Streckeisen, A.L., 1991, The IUGS systematics of igneous rocks: Journal of the Geological Society, v. 148, p. 825–833, https://doi.org/10.1144/gsjgs.148.5.0825.

Le Bas, M.J., Le Maitre, R.W., Streckeiser, A., and Zanettin, B., 1986, Chemical classification of volcanic rocks based on total alkali-silica diagram: Journal of Petrology, v. 27, p. 745–750, https://doi.org/10.1093/petrology/27.3.745.

Le Maitre, R.W., 1976, The chemical variability of some common igneous rocks: Journal of Petrology, v. 17, p. 589–598, https://doi.org/10.1093/petrology/17.4.589.

Le Maitre, R.W., Streckeisen, A.L., Zanettin, B., Le Bas, M.J., Bonin, B., and Bateman, P., eds., 2002, Igneous Rocks: A Classification and Glossary of Terms: Cambridge, UK, Cambridge University Press, 236 p., https://doi.org/10.1017/CBO9780511535581.

Love, J.D., 1939, Geology along the southern margin of the Absaroka Range, Wyoming: Geological Society of America Special Paper 20, 134 p., https://doi.org/10.1130/SPE20-p1.

Love, J.D., 1947, Tertiary stratigraphy of the Jackson Hole area, northwestern Wyoming: U.S. Geological Survey Oil and Gas Investigations Preliminary Chart 27.

Love, J.D., and Love, J.M., 1983, Geologic road log, Jackson to Dinwoody and return: Wyoming Geological Survey Public Information Circular 20, 46 p.

Love, J.D., Christiansen, A.C., Brown, T.M., and Earle, J.L., 1979, Preliminary geologic map of the Thermopolis 1° × 2° quadrangle, central Wyoming: U.S. Geological Survey Open-File Report 79-962, scale 1:250,000.

Machette, M.N., Pierce, K.L., McCalpin, J.P., Haller, K.M., and Dart, R.L., 2001, Map and data for Quaternary faults and folds in Wyoming: U.S. Geological Survey Open-File Report 01-461, 154 p., scale 1:750,000.

McDougall, I., and Harrison, T.M., 1999, Geochronology and Thermochronology by the $^{40}Ar/^{39}Ar$ Method (second edition): New York, Oxford University Press, 269 p.

Mertzman, S.A., 2000, K-Ar results from the southern Oregon–northern California Cascade Range: Oregon Geology, v. 62, p. 99–122.

Mertzman, S.A., 2015, XRF Laboratory: Overview and analytical procedures: http://www.fandm.edu/earth-environment/laboratory-facilities/instrument-use-and-instructions (accessed 21 March 2017).

Meyers, J.B., Rosendahl, B.R., Harrison, C.G.A., and Zan-Dong, D., 1998, Deep-imaging seismic and gravity results from the offshore Cameroon Volcanic Line, and speculation of African hotlines: Tectonophysics, v. 284, p. 31–63, https://doi.org/10.1016/S0040-1951(97)00173-X.

Mirnejad, H., and Bell, K., 2006, Origin and source evolution of the Leucite Hills lamproites: Evidence from Sr-Nd-Pb-O isotopic compositions: Journal of Petrology, v. 47, p. 2463–2489, https://doi.org/10.1093/petrology/egl051.

Morgan, L.A., and McIntosh, W.C., 2005, Timing and development of the Heise volcanic field, Snake River Plain, Idaho, western USA: Geological Society of America Bulletin, v. 117, p. 288–306, https://doi.org/10.1130/B25519.1.

Mueller, P.A., and Wooden, J.L., 1988, Evidence for Archean subduction and crustal recycling, Wyoming province, USA: Geology, v. 16, p. 871–874, https://doi.org/10.1130/0091-7613(1988)016<0871:EFASAC>2.3.CO;2.

Naeser, C.W., Izett, G.A., and Obradovich, J.D., 1980, Fission-track and K-Ar ages of natural glasses: U.S. Geological Survey Bulletin 1489, 31 p.

Niu, Y.L., and O'Hara, M.J., 2003, Origin of ocean island basalts: A new perspective from petrology, geochemistry, and mineral physics considerations: Journal of Geophysical Research, v. 108, 2209, https://doi.org/10.1029/2002JB002048.

Obrebski, M., Allen, R.M., Pollitz, F., and Hung, S., 2011, Lithosphere-asthenosphere interaction beneath the western United States from the joint inversion of body-wave traveltimes and surface-wave phase velocities: Geophysical Journal International, v. 185, p. 1003–1021, https://doi.org/10.1111/j.1365-246X.2011.04990.x.

Payne, S.J., McCaffrey, R., King, R.W., and Kattenhorn, S.A., 2012, A new interpretation of deformation rates in the Snake River Plain and adjacent basin and range regions based on GPS measurements: Geophysical Journal International, v. 189, p. 101–122, https://doi.org/10.1111/j.1365-246X.2012.05370.x.

Pierce, K.L., and Morgan, L.A., 1992, The track of the Yellowstone hotspot: Volcanism, faulting, and uplift, *in* Link, P.K., Kuntz, M.A., and Platt, L.B., eds., Regional Geology of Eastern Idaho and Western Wyoming: Geological Society of America Memoir 179, p. 1–54, https://doi.org/10.1130/MEM179-p1.

Pierce, K.L., and Morgan, L.A., 2009, Is the track of the Yellowstone hotspot driven by a deep mantle plume?—Review of volcanism, faulting, and uplift in light of new data: Journal of Volcanology and Geothermal Research, v. 188, p. 1–25, https://doi.org/10.1016/j.jvolgeores.2009.07.009.

Price, K.B., 2009, Geology of the northern end of the Big Hole Mountains, Madison and Teton County, Idaho [M.S. thesis]: Pocatello, Idaho State University, 120 p.

Protska, H.J., Antweiler, J.C., Bieniewski, C.L., and Kleinkopf, M.D., 1979, Mineral resources of the Du Noir Addition, Washakie Wilderness, Fremont County, Wyoming: U.S. Geological Survey Bulletin 1472, 35 p.

Ray, R.R., and Keefer, W.R., 1985, Wind River Basin, central Wyoming, *in* Gries, R.R., and Dyer, R.C., eds., Seismic Exploration of the Rocky Mountain Region: Denver, Rocky Mountain Association of Petroleum Geologists and Denver Geophysical Society, p. 201–212.

Renne, P.R., Mundil, R., Balco, G., Min, K., and Ludwig, K.R., 2010, Joint determination of ^{40}K decay constants and $^{40}Ar^*/^{40}K$ for the Fish Canyon sanidine standard, and improved accuracy for $^{40}Ar/^{39}Ar$ geochronology: Geochimica et Cosmochimica Acta, v. 74, p. 5349–5367, https://doi.org/10.1016/j.gca.2010.06.017.

Rock, N.M.S., 1977, The nature and origin of lamprophyres: Some definitions, distinctions, and derivations: Earth-Science Reviews, v. 13, p. 123–169, https://doi.org/10.1016/0012-8252(77)90020-4.

Rodgers, D.W., Hackett, W.R., and Ore, H.T., 1990, Extension of the Yellowstone plateau, eastern Snake River Plain, and Owyhee plateau: Geology, v. 18, p. 1138–1141, https://doi.org/10.1130/0091-7613(1990)018<1138:EOTYPE>2.3.CO;2.

Rodgers, D.W., Ore, H.T., Bobo, R.T., McQuarrie, N., and Zentner, N., 2002, Extension and subsidence of the eastern Snake River Plain, Idaho, *in* Bonnichsen, B., White, C.M., and McCurry, M., eds., Tectonic and Magmatic Evolution of the Snake River Plain Volcanic Province: Idaho Geological Survey Bulletin 30, p. 121–155.

Rohrer, W.L., 1966, Geologic map of the Kisinger Lakes quadrangle, Fremont County, Wyoming: U.S. Geological Survey Quadrangle Map GQ-527, scale 1:24,000.

Rohrer, W.L., and Obradovich, J.D., 1978, Age of volcanism at Togwotee Pass area in Wyoming: U.S. Geological Survey Professional Paper 1100, p. 183.

Rudnick, R.L., and Gao, S., 2003, Composition of the continental crust, *in* Rudnick, R.L., Treatise on Geochemistry, Volume 3: The Crust: Oxford, UK, Pergamon, p. 1–64.

Sears, J.W., Hendrix, M.S., Thomas, R.C., and Fritz, W.J., 2009, Stratigraphic record of the Yellowstone hotspot track, Neogene Sixmile Creek Formation grabens, southwest Montana: Journal of Volcanology and Geothermal Research, v. 188, p. 250–259, https://doi.org/10.1016/j.jvolgeores.2009.08.017.

Seeland, D.A., and Brauch, E.F., 1975, Status of mineral resource information for the Wind River Indian Reservation, Wyoming: U.S. Geological Survey and United States Bureau of Mines Administrative Report BIA-8, 66 p.

Shervais, J.W., and Hanan, B.B., 2008, Lithospheric topography, tilted plumes, and the track of the Snake River–Yellowstone hot spot: Tectonics, v. 27, TC5004, https://doi.org/10.1029/2007TC002181.

Sleep, N.H., 2003, Fate of mantle plume material trapped within a lithospheric catchment with reference to Brazil: Geochemistry Geophysics Geosystems, v. 4, 8509, https://doi.org/10.1029/2002GC000464.

Smith, R.B., Jordan, M., Steinberger, B., Puskas, C.M., Farrell, J., Waite, G.P., Husen, S., Chang, W.-L., and O'Connell, R., 2009, Geodynamics of the Yellowstone hotspot and mantle plume: Seismic and GPS imaging, kinematics, and mantle flow: Journal of Volcanology and Geothermal Research, v, 118, p. 26–56, https://doi.org/10.1016/j.jvolgeores.2009.08.020.

Smithies, R.H., Champion, D.C., and Sun, S.-S., 2004, Evidence for early LREE-enriched mantle source regions: Diverse magmas from the c. 3.0 Ga Mallina Basin, Pilbara Craton, NW Australia: Journal of Petrology, v. 45, p. 1515–1537, https://doi.org/10.1093/petrology/egh014.

Steidtmann, J.R., and Middleton, L.T., 1991, Fault chronology and uplift history of the southern Wind River Range, Wyoming: Implications for Laramide and post-Laramide deformation in the Rocky Mountain Fault chronology and uplift history of the southern Wind River Range, Wyoming: Geological Society of America Bulletin, v. 103, p. 472–485, https://doi.org/10.1130/0016-7606(1991)103<0472:FCAUHO>2.3.CO;2.

Sun, S.-s., and McDonough, W.F., 1989, Chemical and isotopic systematics of oceanic basalts: Implications for mantle composition and processes, *in* Saunders, A.D., and Norry, M.J., eds., Magmatism in the Ocean Basins: Geological Society of London Special Publication 42, p. 313–345, https://doi.org/10.1144/GSL.SP.1989.042.01.19.

Takada, A., 1994, The influence of regional stress and magmatic input on styles of monogenetic and polygenetic volcanism: Journal of Geophysical Research, v. 99, p. 13,563–13,574, https://doi.org/10.1029/94JB00494.

Vogl, J.J., Min, K., Carmenate, A., Foster, D.A., and Marsellos, A., 2014, Miocene regional hotspot-related uplift, exhumation, and extension north of the Snake River Plain: Evidence from apatite (U-Th)/He thermochronology: Lithosphere, v. 6, p. 108–123, https://doi.org/10.1130/L308.1.

Wegmann, K.W., Zurek, B.D., Regalla, C.A., Bilardello, D., Wollenberg, J.L., Kopczynski, S.E., Ziemann, J.M., Haight, S.L., Apgar, J.D., Zhao, C., and Pazzaglia, F.J., 2007, Position of the Snake River watershed divide as an indicator of geodynamic processes in the greater Yellowstone region, western North America: Geosphere, v. 3, p. 272–281, https://doi.org/10.1130/GES00083.1.

Winterfeld, G.F., and Conard, J.B., 1983, Laramide tectonics and deposition, Washakie Range and northwestern Wind River Basin, Wyoming, *in* Lowell, J.D. and Gries, R., eds., Rocky Mountain Foreland Basins and Uplifts: Denver, Colorado, Rocky Mountain Association of Geologists, p. 137–148.

Woolley, A.R., Bergman, S.C., Edgar, A.D., Le Bas, M.J., Mitchell, R.H., Rock, N., and Smith, B., 1996, Classifications of lamprophyres, lamproites, kimberlites, and the kalsilitic, melilitic, and leucite rocks: Canadian Mineralogist, v. 34, p. 175–186.

Yonkee, W.A., and Weil, A.B., 2015, Tectonic evolution of the Sevier and Laramide belts within the North American Cordillera orogenic system: Earth-Science Reviews, v. 150, p. 531–593, https://doi.org/10.1016/j.earscirev.2015.08.001.

York, D., Hall, C.M., Yanase, Y., Hanes, J.A., and Kenyon, W.J., 1981, $^{40}Ar/^{39}Ar$ dating of terrestrial minerals with a continuous laser: Geophysical Research Letters, v. 8, p. 1136–1138, https://doi.org/10.1029/GL008i011p01136.